Transverse emittance growth due to rf noise in crab cavities: Theory, measurements, cure, and high luminosity LHC estimates

P. Baudrenghien
CERN, Geneva 1211, Switzerland

T. Mastoridis
California Polytechnic State University, San Luis Obispo, California, USA

(Received 5 June 2023; accepted 12 April 2024; published 6 May 2024)

The High-Luminosity LHC (HL-LHC) upgrade with planned operation from 2029 onward has a goal of achieving a tenfold increase in the integrated number of recorded collisions thanks to a doubling of the intensity per bunch (2.2×10^{11} protons) and a reduction of β^* (the β value in the two high luminosity detectors, namely ATLAS and CMS) to 15 cm. Such an increase in recorded collisions would significantly expedite new discoveries and exploration. Crab cavities are an important component of the HL-LHC upgrade and will contribute strongly to achieving an increase in the number of recorded collisions. However, noise injected through the crab cavity radio frequency (rf) system could cause significant transverse emittance growth and limit luminosity lifetime. We presented a theoretical formalism relating transverse emittance growth to rf noise in an earlier work. In this follow-up paper, we summarize measurements in the super-proton synchrotron (SPS) at CERN that validate the theory, we present estimates of the emittance growth rates using state-of-the-art rf and low-level rf (LLRF) technologies, and we set the rf noise specifications to achieve acceptable performance. A novel dedicated feedback system acting through the crab cavities to mitigate emittance growth will be required. In this work, we develop a theoretical formalism to evaluate the performance of such a feedback system in any collider, identify limiting components, present simulation results to validate these studies, and derive key design parameters for an HL-LHC implementation of such a feedback system.

DOI: 10.1103/PhysRevAccelBeams.27.051001

I. INTRODUCTION

In the nominal LHC, opposing bunches cross each other at an angle, rather than head-on, causing a luminosity reduction factor of up to 20%. Thanks to the recent upgrade of the LHC injector chain (LIU), the HL-LHC will double the LHC intensity per bunch to about 2.2×10^{11} protons in stable beams–the LHC mode during collisions and data taking. To avoid detrimental effects from long-range beam-beam interactions due to the increased beam intensity, the half crossing angle must be increased to 250 μrad from the beginning of collisions. Without bunch crabbing, this large crossing angle and small transverse beam size would result in a luminosity reduction factor of 0.3 (Piwinski reduction factor) [1]. Therefore, crab cavities are an important component of the LHC upgrade and will contribute strongly to achieving an increase in the number of recorded collisions [2].

The proposed crab cavities are electromagnetic devices with a resonant frequency of 400.789 MHz. They cause a kick perpendicular to the direction of motion (transverse kick), as shown in Fig. 1. The rf kick is centered on the bunch longitudinal core. Thus, the head and tail receive kicks in opposite directions, thereby resulting in a transverse bunch rotation (crabbing) and a more head-on collision between the particle beams [3]. The HL-LHC will use a "local" crabbing scheme. The crabbing is

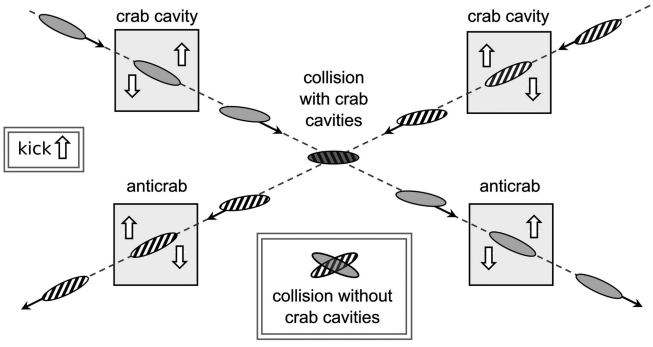

FIG. 1. Crab cavity induced bunch rotation [7].

localized around interaction point (IP) 1 (ATLAS) and IP 5 (CMS). Outside these experiments, there is no bunch rotation. The crab cavities are located at about a 90° betatron phase advance with respect to the IP. Crab cavities have also been developed, installed, and operated at KEKB [4–6].

Crab cavities have not been used in hadron colliders before. Noise injected through the rf system could cause significant transverse emittance growth and limit luminosity lifetime [8]. Thus, rf noise presents a significant challenge in the collider operation with crab cavities. Section II summarizes the theoretical formalism previously derived by the authors, relating the rf noise to transverse emittance growth, as well as its extension when there is a coupling between the two transverse planes. Section III presents the validation at the SPS, as well as the effects of coupling with the transverse impedance. Crab cavity rf noise thresholds for the HL-LHC are estimated using the presented theory and are shown in Sec. IV. Section V estimates the noise levels of the proposed crab cavity low-level rf (LLRF) system. Section VI presents a novel feedback system that will act through the crab cavities to reduce the effect of rf noise on transverse emittance growth. Analytical expressions are derived to calculate the emittance growth reduction achieved with this proposed feedback system, as a function of the system gain, delay, and beam pickup measurement noise levels. These expressions can be used to evaluate the effectiveness of this novel feedback system in other accelerators employing crab cavities, such as the Electron-Ion Collider (EIC). Section VII includes the simulation results of this proposed feedback system. Finally, in Sec. VIII, we use the analytical expressions derived in this work to design the optimal feedback system for the HL-LHC case and set specifications for the pickup measurement noise level.

II. TRANSVERSE EMITTANCE GROWTH DUE TO RF NOISE

A. Summary of previous work by the authors

The emittance growth rate due to phase and amplitude noise was derived by the authors in [9]. The equations below give the transverse emittance growth, in the plane of crabbing, caused by the rf phase and amplitude noise of a single crab cavity. They were derived analytically and validated through extensive simulations in [9] and [10].

$$\frac{d\epsilon_n}{dt} = \gamma\beta_{cc}\left(\frac{eV_o f_{\mathrm{rev}}}{2E_b}\right)^2 C_{\Delta\phi}(\sigma_\phi) \times \sum_{p=-\infty}^{\infty} S_{\Delta\phi}[(p \pm \bar{\nu}_b) f_{\mathrm{rev}}]$$

$$C_{\Delta\phi}(\sigma_\phi) = e^{-{\sigma_\phi}^2}\left[I_o({\sigma_\phi}^2) + 2\sum_{l=1}^{\infty} I_{2l}({\sigma_\phi}^2)\right], \quad (1)$$

$$\frac{d\epsilon_n}{dt} = \gamma\beta_{cc}\left(\frac{eV_o f_{\mathrm{rev}}}{2E_b}\right)^2 C_{\Delta A}(\sigma_\phi) \times \sum_{p=-\infty}^{\infty} S_{\Delta A}[(p \pm \bar{\nu}_b \pm \bar{\nu}_s) f_{\mathrm{rev}}]$$

$$C_{\Delta A}(\sigma_\phi) = e^{-{\sigma_\phi}^2}\sum_{l=0}^{\infty} I_{2l+1}({\sigma_\phi}^2), \quad (2)$$

where ϵ_n is the normalized horizontal transverse emittance (assuming a horizontal crabbing scheme. Equations hold for vertical emittance in case of vertical crabbing), β_{cc} is the beta function at the crab cavity location (in m), e is the charge of a proton, V_o is the voltage of the crab cavity, f_{rev} is the revolution frequency, E_b the beam energy, σ_ϕ the rms bunch length (in radians with respect to the rf frequency), I is the modified Bessel function of the first kind, $\bar{\nu}_b$ is the noninteger betatron tune averaged over the particles, $\bar{\nu}_s$ is the mean synchrotron tune, and $S_{\Delta\phi}$, $S_{\Delta A}$ are the phase and (relative) amplitude noise power spectral density (PSD), respectively (with units of rad^2/Hz and 1/Hz respectively). The voltage PSD is $S_{\Delta V} = V_o^2 S_{\Delta A}$. The $\pm$ sign refers to upper and lower sidebands. As the crab cavity rf has zero phase at the center of the bunch, phase noise kicks lead to a shift of the bunch's centroid position at the IP, whereas amplitude noise leads to a rotation of the bunch around its centroid. These expressions correspond to *one* crab cavity. The total emittance growth scales linearly with the number of crab cavities, assuming uncorrelated noise. This is a reasonable assumption in the HL-LHC case due to the noise sources presented in Sec. V.

The factors $C_{\Delta\phi}(\sigma_\phi)$ and $C_{\Delta A}(\sigma_\phi)$ correspond to normal distributed bunches and express the effect of bunch length on the transverse emittance growth. They are the only factors in these Equations that are distribution dependent. Appendix A presents $C_{\Delta\phi}(\sigma_\phi)$ for a pillbox distribution in the longitudinal phase space and shows only a small deviation from the two-dimensional Gaussian case above. Since the two factors do not change much between these two extreme distributions, it is safe to assume that there won't be a significant change for any commonly encountered distribution.

From Eqs. (1) and (2), it is clear that the emittance growth depends on accelerator parameters, the bunch length [$C_{\Delta\phi}(\sigma_\phi)$ and $C_{\Delta A}(\sigma_\phi)$], and the noise PSD sampled at the betatron or synchrobetatron sidebands of all revolution harmonics. The emittance growth rate depends on the bunch length because the HL-LHC bunch length (1 ns 4σ) is a significant portion of the rf period (2.5 ns), so the momentum kicks from the crab cavities are not simply proportional to the z position of the particles.

The phase noise emittance growth rate is reduced by the LHC transverse damper by a correction factor of $\overline{R_d}$ [9].

$$\overline{R_d} = \frac{1}{\pi}\int_{-\infty}^{\infty} g(u)\left\{1 - \frac{e^{-\sigma_\phi^2}}{C_{\Delta\phi}(\sigma_\phi)}\frac{\alpha^2[g(u)^2 + f(u)^2] + 2\alpha g(u)}{[1+\alpha g(u)]^2 + [\alpha f(u)]^2}\right\}du$$
$$\alpha = \frac{G}{4\pi\sigma_{\nu_b}}, \tag{3}$$

where G is the LHC transverse damper gain, σ_{ν_b} is the rms betatron tune spread, and $f(u)$, $g(u)$ are scaled versions of the real and imaginary parts of the transverse beam transfer function, which is derived from the tune distribution $\rho(\nu_b)$ [9]. In this work, we use a distribution $\rho_{\mathrm{sim}}(\nu_b)$ dominated by head-on beam-beam effects, with smaller, but not insignificant chromaticity contributions, as expected for the HL-LHC in stable beams. This tune distribution is shown in Fig. 12 in [9]. The correction factor has some dependence on the assumed tune distribution (up to 20%), as shown in Fig. 8 in [9].

The damper is not efficient for long bunches because it applies the same kick for all particles in the bunch, whereas the phase noise kick is cosinusoidal. In addition, the LHC damper acts bunch-by-bunch and thus cannot reduce amplitude noise effects since they do not affect the mean bunch position.

B. Transverse emittance growth rates with *x-y coupling*

The expressions in [9] were derived assuming no coupling between the two transverse planes. In the presence of coupling, the noise effect is shared between the two planes so that the scaled noise power in the right-hand side of Eqs. (1) and (2) is now equal to the sum of the horizontal and vertical growth rates.

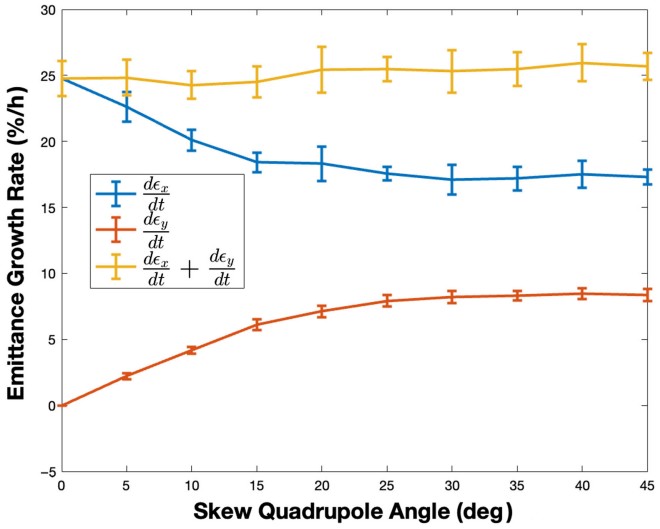

FIG. 2. Horizontal and vertical emittance growth rates as a function of the skew quadrupole angle.

The ratio of the horizontal and vertical growth rates depends on the coupling strength. This was tested in simulations by modeling the action of a skew quadrupole magnet. The growth rate ratio changes as the skew angle of a quadrupole magnet is varied, as expected. The sum of the growth rates remained constant for all skew settings though, as seen in Fig. 2. This relationship was tested for various magnet strengths.

This coupling between the two planes is inconsequential for the HL-LHC since crabbing will be on two different planes at IP1 and IP5. Since the crabbing voltage, the β_{cc}, and the rf/LLRF design will be identical for the two IPs, the sum of the emittance growth rate contributions from the two IPs will be constant in both planes.

III. COUPLING WITH TRANSVERSE IMPEDANCE AND SPS VALIDATION

Two prototype LHC crab cavities (double quarter wave type) were installed in the SPS in 2017 to measure their impact on a high intensity proton beam [11]. A machine development session was conducted on September 5, 2018, in the SPS to measure transverse emittance growth rates due to crab cavity noise. Unfortunately, only one crab cavity was available operating at just one-third of the maximum voltage, which limited the range of possible measurements. Still, it was very helpful to get some data to further validate the theory summarized in Sec. II. Over the course of 7 h, there were four different beam coasts with eight total different periods of controlled phase noise excitation and bunch measurements (two of those periods were without any additional injected noise and were used to estimate background emittance growth). These measurements confirmed the functional dependence of emittance growth on rf noise but had a constant scaling error of about 3.4, as seen in Fig. 3 [12].

There was no opportunity for further measurements in the SPS until 2022 due to the LHC Long Shutdown 2. In the meantime, we investigated various possible reasons for this discrepancy, including (i) beam losses that would lead to an emittance reduction, (ii) changes in the transverse distribution due to the crab cavity noise that would lead to inaccurate emittance measurements (for example, high tail population below the measurement noise floor), (iii) coupling between the horizontal and vertical planes, and (iv) bunch length and longitudinal distribution variations that would affect $C_{\Delta\phi}(\sigma_\phi)$ and $C_{\Delta A}(\sigma_\phi)$. None of these provided a convincing explanation.

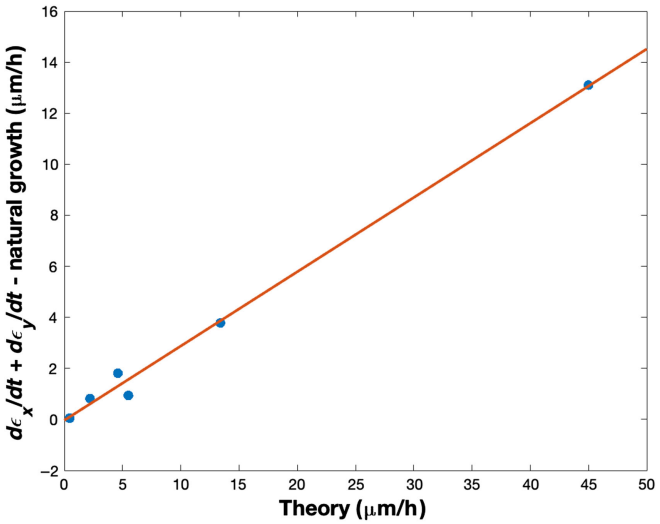

FIG. 3. Measured and expected emittance growth rates.

An alternative mechanism was suggested. The equations presented in Sec. II assume that the transverse filamentation is fast enough so that the noise kicks result in emittance growth rather than a coherent transverse beam oscillation. This assumption is valid for the HL-LHC in stable beams since the decoherence time is less than a second while the coast typically lasts for several hours. Coupling with the transverse impedance can, however, shift the coherent betatron tune outside of the incoherent tune spectrum and thus lead to suppression of the emittance growth. Part of the noise power drives the coherent betatron oscillation, without emittance growth in the presence of transverse damping. Past literature has similarly shown that head-on beam-beam effects convert part of the excitation noise to a coherent π-mode oscillation [13,14].

This mechanism was studied [15] and confirmed via simulations and through measurements in the SPS at CERN in 2022 [16,17]. During these measurements, the octupole strength and thus the tune spread was increased. As a result, the coherent tune increasingly overlapped with the incoherent tune spectrum, and the suppression of the emittance growth was reduced. For high octupole strengths, when the coherent tune is inside the incoherent tune spread, the measured growth rates agreed with the analytical prediction [18].

This suppression mechanism will *not* be present in the HL-LHC. The coherent betatron tune is not expected to shift outside the incoherent tune spectrum [19]. In stable beams, the beam-beam interactions lead to significant tune spread, which will include the coherent tune. Therefore, this suppression mechanism should not have a measurable effect and is not included in this study.

There are very limited data from the SPS measurements in 2022 with only amplitude noise. More measurements with amplitude noise are planned in 2025 or 2026.

IV. CRAB CAVITY RF NOISE THRESHOLDS

The HL-LHC has a target of 1% integrated luminosity loss due to crab cavity induced transverse emittance growth. The transverse emittance growth rate is a function of parameters that change significantly during the HL-LHC cycle.

A. HL-LHC parameters

The HL-LHC is intended to operate the crab cavities with a fixed $V_o = 3.4$ MV (per cavity) during collisions. A full crossing angle θ_c of 380 μrad will be applied from the beginning of stable beams. A total voltage of 6.8 MV is required to achieve this, so the HL-LHC local crabbing scheme contains two crabbing cavities and two uncrabbing cavities per IP and per beam. Each cavity pair shares a cryostat and is located about 150 m from the IP. One transverse pickup will be placed next to each cavity pair, in the plane of crabbing (two pickups per plane and per beam) [2].

The HL-LHC will also employ $\beta^\star$ leveling: $\beta^\star$ will be reduced from 0.64 to 0.15 m during stable beams [20] which in turn leads to an increase of β_{cc} for a constant full crossing angle and voltage ($\beta_{cc} = 3620$ m at the end of the fill). As a result, the transverse emittance growth rate due to crab cavity noise will increase during the fill and will be maximized at the end of the stable beams mode (minimum β^*).

The actual β^* leveling procedure might be adjusted before HL-LHC starts operating. Options considered include starting collisions with β^* larger than 0.64 m or terminating collisions with a β^* of 0.18 m. In all cases, the final value at the end of the cycle will be 0.15 m or more. In this work, we use 0.15 m, which leads to the most challenging transverse emittance growth rate and is thus a conservative estimate.

Before the start of stable beams, crabbing is not needed nor desired, and thus there is an option to keep the crab cavities off. This is not ideal, because then there is no control of the cavity tune, which could intersect a betatron line during the acceleration ramp leading to transverse instabilities. Alternatively, the crab cavities can be kept on at a reduced voltage (300 kV) during filling and ramping, with counterphasing on (the layout includes two crab cavities per beam and per IP side [2]), as they have sufficient tuning range so that the total crabbing voltage is zero while maintaining active control of cavity tune and field. This is the current operational scenario.

The HL-LHC operational parameters are currently being finalized [20]. Early estimates of those parameters are used in this work and are summarized in Table I. Additionally, the HL-LHC beam is defined as 7.61 cm rms bunch length for a q-Gaussian distribution with $q = \frac{3}{5}$ [21], 25 ns bunch spacing, 2.2×10^{11} protons per bunch, and 2760 bunches per beam, amounting to 1.09 A dc. A horizontal and

TABLE I. Nominal HL-LHC parameters in stable beams.

f_{rev} (Hz)	ν_x	f_{rf} (MHz)	V_o (MV)	θ_c (μrad)	ϵ_n (μm rad)	E_b (TeV)	σ_ϕ (rad)	σ_{ν_b}
11, 245	62.31	400.789	3.4	380	2.5	7	0.67	0.003

vertical rms betatron tune spread of 0.003 is used. Four crab cavities per beam and per plane (horizontal, vertical) are included in these estimates.

B. Emittance growth threshold

Equations (1) and (2) include a scaling factor that depends on the operational scheme and parameters summarized above, defined as

$$C_{\mathrm{OP}} = \gamma\beta_{cc}\left(\frac{eV_o f_{\mathrm{rev}}}{2E_b}\right)^2.$$

The factor C_{OP} changes significantly during the acceleration ramp and is shown in Fig. 4 during the nominal HL-LHC cycle. Clearly, the end of stable beams (the part of the cycle with the minimum β^*) is the most critical period. It is also interesting to note that the crab cavity noise effects during the injection and energy ramp are inconsequential.

This rf noise scaling was used in [21] to set a 2%/hour emittance growth threshold with the lowest β^* (15 cm) optics at the end of the stable beams mode. This growth rate achieves the 1% integrated luminosity target and sets a limit on the crab cavity noise level.

C. Aliased noise power spectrum

Equations (1)–(3) can then be used to estimate the corresponding threshold on the noise power. For phase noise [Eq. (1)], the noise power is the sum of the phase noise PSD sampled on all betatron sidebands (two per revolution frequency line). For amplitude noise [Eq. (2)], we must sum the amplitude noise PSD on all synchrobetatron sidebands (four per revolution frequency line).

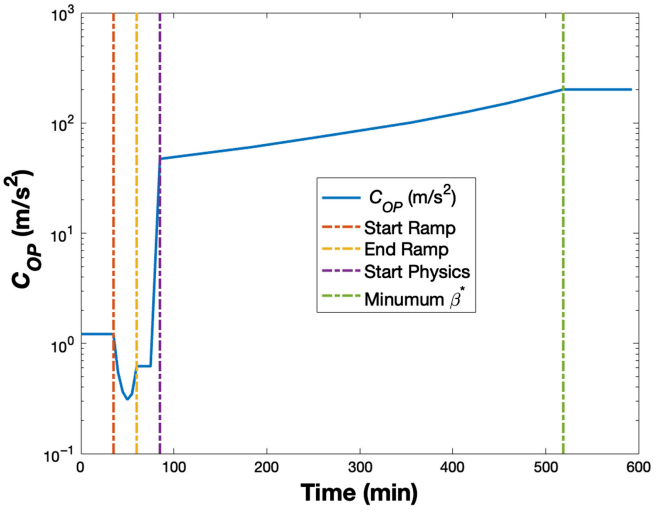

FIG. 4. rf noise scaling during the HL-LHC cycle.

Equations (1) and (2) consider the continuous-time situation where the bunch samples the noise at every turn. In the frequency domain, this results in an aliased noise spectrum. This suggests the introduction of an effective PSD—used to compute the emittance growth rate—defined as

$$\sum_{p=-\infty}^{\infty} S_{\Delta\phi}[(p \pm \bar{\nu}_b) f_{\mathrm{rev}}] = 2S_{\Delta\phi,\mathrm{eff}}(\bar{\nu}_b f_{\mathrm{rev}}), \tag{4}$$

$$\sum_{p=-\infty}^{\infty} S_{\Delta A}[(p \pm \bar{\nu}_b \pm \bar{\nu}_s) f_{\mathrm{rev}}] = 4S_{\Delta A,\mathrm{eff}}(\bar{\nu}_b f_{\mathrm{rev}}). \tag{5}$$

$S_{\Delta\phi,\mathrm{eff}}(f)$, $S_{\Delta A,\mathrm{eff}}(f)$ are the *aliased* PSDs extending from $-f_{\mathrm{rev}}/2$ to $f_{\mathrm{rev}}/2$ that lead to the same total noise power sampled by the beam. Note that $S(f)$ is even symmetric as any PSD.

The beam only reacts to the noise power on a narrow band (tune distribution) around the betatron sidebands. We define this phase and amplitude noise power as $\sigma^2_{\Delta\phi}$ and $\sigma^2_{\Delta A}$. $\sigma^2_{\Delta V}$ is the corresponding amplitude noise power per cavity. Then,

$$2S_{\Delta\phi,\mathrm{eff}}(\bar{\nu}_b f_{\mathrm{rev}}) = 2\frac{\sigma^2_{\Delta\phi}}{f_{\mathrm{rev}}}, \tag{6}$$

$$4S_{\Delta A,\mathrm{eff}}(\bar{\nu}_b f_{\mathrm{rev}}) = 4\frac{\sigma^2_{\Delta A}}{f_{\mathrm{rev}}} = 4\frac{\sigma^2_{\Delta V}}{f_{\mathrm{rev}} V_o^2}. \tag{7}$$

D. rf noise threshold

The threshold on the "effective" noise power can be translated to an rf noise threshold using the planned LLRF architecture and associated noise sources. In the HL-LHC, the crabbing and uncrabbing cavities are 300 m apart and thus it is not possible to share a power source, LLRF, etc. Since each cavity has its own LLRF, the noise will be uncorrelated among cavities. Therefore, the total noise contributions are added in power, leading to a linear scaling of the emittance growth rate with the number of crab cavities. Since the I/Q demodulator is the dominant noise source (Sec. V), we can assume that $S_{\Delta\phi}(f) = S_{\Delta A}(f)$.

Using Equations (1)–(5), the HL-LHC parameters defined in IV A, and the emittance growth rate threshold from IV B, we can evaluate the rf noise thresholds

including the reduction provided by the transverse damper: $S_{\Delta\phi,\mathrm{eff}}(f) = 0.0171\ (\mu\mathrm{rad})^2/\mathrm{Hz}$ and $S_{\Delta A,\mathrm{eff}}(f) = 0.0171 \times 10^{-12}$ 1/Hz. These rf noise thresholds, applied to each cavity, lead to an emittance growth rate of 0.92%/h and 1.08%/h due to phase and amplitude noise, respectively, with the four cavities per beam and plane.

Even though the effective PSD is the same for phase and amplitude noise, the bunch length factors are significantly different ($C_{\Delta\phi}(\sigma_\phi) = 0.72$ and $C_{\Delta A}(\sigma_\phi) = 0.14$). In addition, the phase noise PSD is sampled at two sidebands and the amplitude noise PSD at four sidebands. Finally, the phase noise effect is reduced by the transverse damper by a factor of $\overline{R_d} = 0.32$ [from Eq. (3)], for the transverse tune distribution described in Sec. II and for $G = 0.04$ (damping time of 50 turns [21]). The transverse damper cannot mitigate amplitude noise, as explained in Sec. II. The total scaling of the noise contributions is thus 0.46 for phase noise and 0.56 for amplitude noise. Their ratio agrees with the ratio of the emittance growth estimates above.

V. HL-LHC CRAB CAVITY RF NOISE SPECTRUM ESTIMATE

An estimate of the crab cavity rf noise power spectrum is necessary to evaluate the rf noise sampled by the beam. This depends on both the high level and low level rf systems, which are currently being designed.

The LLRF has to reduce the crab cavity impedance at the resonance (400.8 MHz) by a factor of at least 1000 (linear) to maintain transverse stability [22]. To achieve this it will include a proportional feedback and a one-turn delay feedback, which will regulate the transmitter drive using a measurement of the cavity field, a common solution for high intensity synchrotrons [23]. The LLRF will use the architecture introduced for the SPS LLRF upgrade [24,25]: fixed frequency clocks—including the demodulator/modulator local oscillator (LO)—transmission of the rf frequency as numerical word via the White Rabbit link, and synchronous demodulation via Numerically Controlled Oscillator (NCO).

The proportional feedback loop delay will be about 1.3 μs, including the transmitter delay (at most 100 ns). This delay limits the gain to 151 (linear) to achieve a 10 dB gain margin for a cavity Q_L of 500,000 and R/Q of 215 Ω, resulting in a closed-loop bandwidth of 136 kHz [26]. The impedance at the resonant frequency is reduced by a factor of 151. The cavity impedance will be further reduced on the betatron sidebands by a factor of ≈10 via the one-turn delay feedback system, leading to a total impedance reduction of ≈1500. The LLRF design is presented in more detail in [23].

We will use the existing LHC rf system as a starting point for the rf noise power spectrum estimate. The phase noise PSD $S_{\Delta\phi}(f)$ measured at the LHC main rf system (accelerating cavities, with a LLRF designed in the early 2000s) is shown in Fig. 5. This is the noise PSD *per cavity*. The asterisks in the figure correspond to the first 40 betatron sidebands. The corresponding $S_{\Delta\phi,\mathrm{eff}}(f)$ is 11.5 $(\mu\mathrm{rad})^2/\mathrm{Hz}$.

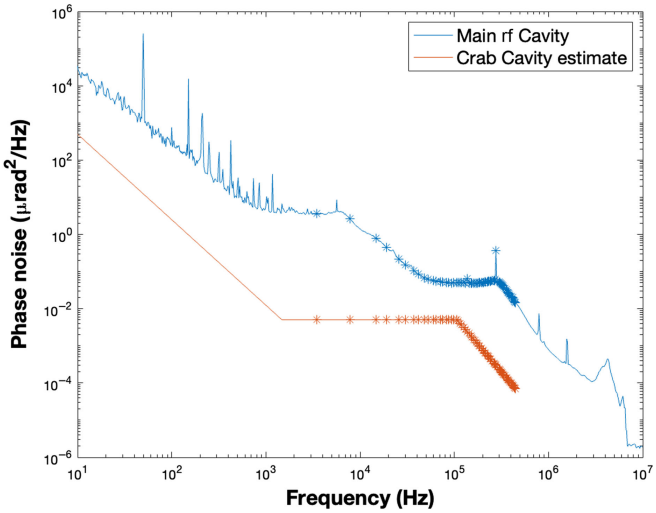

FIG. 5. LHC main accelerating cavity (measured) and crab cavity (estimated) phase noise.

The crab cavity noise spectrum is dominated by rf/LLRF sources, such as the transmitter, clock distribution, and demodulator. Figure 5 compares the LHC main rf noise spectrum with the HL-LHC crab cavity estimate, which includes *significant* improvements [23]: (i) The bump between 1 and 40 kHz in the main rf cavity PSD has been traced to the phase noise in the demodulating LO. This will not be present in the crab cavities: thanks to the fixed-frequency clocks and LO, we will use narrow band phase-lock loops, thus improving the demodulator LO and thereby reducing the rf phase noise at the first two betatron sidebands below the demodulator level. The spectrum will remain flat in the 1–40 kHz range. (ii) Using inductive output tubes (IOT) instead of klystrons, hereby reducing transmitter noise. This noise will be further reduced by the feedback gain, within the closed loop bandwidth. (iii) We will use analog-to-digital converters with a higher effective number of bits, thus reducing the rf demodulator noise by at least 10 dB.

With these improvements, we anticipate that the noise spectrum will be dominated by the demodulator, resulting in a flat noise spectrum within the closed loop bandwidth.

The loop delay is much higher for the crab cavity LLRF (1.3 μs) than for the main accelerating cavities (650 ns), due to the relative location of the cavities, LLRF, and the transmitters. Therefore, the noise spectrum bandwidth is about half as much for the crab cavities.

As a result, the expected $S_{\Delta\phi,\mathrm{eff}}(f)$ is reduced to 0.141 $(\mu\mathrm{rad})^2/\mathrm{Hz}$, still more than a factor of 8 higher than the defined threshold, which would result in an unacceptable 16.6%/h emittance growth rate (7.6%/h due to phase and 9.0%/h due to amplitude noise) with the four cavities per beam and plane. The 7.6%/h rate due to

phase noise includes the transverse damper reduction factor of $\overline{R_d} = 0.32$. Without the damper, the rate would be 23.7%/h.

The HL-LHC crab cavity rf noise levels are clearly too high. Even with the planned significant architectural and technological improvements to significantly reduce the noise compared to the LHC accelerating cavities, the anticipated HL-LHC crab cavity rf noise levels will still be higher than the threshold and will greatly reduce the HL-LHC performance. Thus, a dedicated feedback system to reduce the effect of crab cavity noise on emittance growth is necessary.

VI. CRAB CAVITY RF NOISE FEEDBACK

Emittance growth caused by crab cavity rf noise is a two-step process. First, noise excites a bunch oscillation. Then, this oscillation results in emittance growth through decoherence due to the betatron tunespread. A feedback system can mitigate this degradation if it damps the oscillation *before* decoherence has significantly impacted the emittance. A novel dedicated feedback system is proposed that would use the *existing* crab cavities as kickers to mitigate rf noise effects. As such, no new kickers or crab cavities will have to be designed. The proposed feedback system could share pickup signals with the existing transverse damper (Fig. 6). The proposed pickup will strongly couple to the bunch head-tail motion and will extract both the dipole (mode 0) and head-tail (mode 1) motion. The crab cavity feedback will also compensate for bunch oscillations caused by other sources within its bandwidth (both common mode and head-tail).

The resulting error signal will be applied directly to the crab cavity voltage set point, in amplitude and phase. Therefore, the crab cavity feedback will be able to act on both phase and amplitude noise with a correction that will be a perfect scaled version of the noise momentum kick—if it is caused by the crab cavity rf noise.

A. Emittance growth reduction with mode 0 feedback

It is important to analytically estimate the effectiveness of the proposed feedback system to evaluate its potential in reducing the emittance growth due to crab cavity rf noise. In [9], we derived expressions for the action of a transverse damper on rf noise effects. The proposed feedback could share a pickup with the transverse damper. However, since it will use the crab cavities as kickers, its response will have the appropriate sinusoidal dependence, whereas the transverse damper applies the same correction to all the particles of a given bunch. We can therefore follow the derivation for the transverse damper (Appendix D in [9]) with the appropriate modifications.

We first consider the effect of a single cavity with voltage V_0. Its phase noise is represented as a sequence of random samples (a statistical process) $\boldsymbol{\Delta\phi}_k$ with turn index k. Consider a particle ζ with betatron tune ν_b, peak amplitude of the synchrotron oscillation $\hat{\phi}$ (in radians), synchrotron tune ν_s, and phase of the synchrotron oscillation at time zero ψ. The phase noise sequence $\boldsymbol{\Delta\phi}_k$ results in a normalized momentum kick sequence $\boldsymbol{\Delta p}_{\phi,k}$. The normalized position shift $\tilde{\boldsymbol{x}}_n$ at turn n is the convolution of the particle response (sinusoid at ν_b) and the momentum kicks

$$\begin{aligned}\tilde{\boldsymbol{x}}_n &= \sum_{k=0}^{n} \sin\left[2\pi\nu_b(n-k)\right]\boldsymbol{\Delta p}_{\phi,k} \\ &= \sqrt{\beta_{cc}}\frac{eV_0}{E_b}\sum_{k=0}^{n}\sin\left[2\pi\nu_b(n-k)\right] \\ &\quad\times\cos\left[\hat{\phi}\cos\left(2\pi\nu_s k+\psi\right)\right]\boldsymbol{\Delta\phi}_k, \end{aligned} \tag{8}$$

where $\tilde{x}_n = \frac{\tilde{X}_n}{\sqrt{\beta}}$ (with $\tilde{X}_n$ the position shift in meter). In the second equation, we have expanded the momentum kick as a cosinusoidal function of the particle phase deviation at turn k. This derivation is presented in [9] with more details.

The mode 0 signal at the crab cavity location at turn n is the ensemble average of $\tilde{\boldsymbol{x}}_n$ for all particles in a bunch. Bold face characters ($\boldsymbol{\nu}_b, \boldsymbol{\nu}_s, \hat{\boldsymbol{\phi}}, \boldsymbol{\psi}, \tilde{\boldsymbol{x}}_n, \boldsymbol{\Delta\phi}_n, \boldsymbol{\Delta A}_n$) are used for random variables and statistical processes. Lower case characters (ν_b, ν_s, $\hat{\phi}$, ψ, $\tilde{x}_n$, $\Delta\phi_n$, ΔA_n) are used for particular values taken by these variables or processes. We use the symbol $E[.]$ for the ensemble average. It is taken over all random variables included within the square brackets. As shown in Appendix D in [9], with some simplifying assumptions concerning the statistical distributions [27]:

$$\begin{aligned}&E\{\sin[2\pi\boldsymbol{\nu}_b(n-k)]\cos[\hat{\boldsymbol{\phi}}\cos(2\pi\boldsymbol{\nu}_s k+\boldsymbol{\psi})]\}\boldsymbol{\Delta\phi}_k \\ &\quad= e^{-\frac{\sigma_\phi^2}{2}}h_{n-k}\boldsymbol{\Delta\phi}_k,\end{aligned} \tag{9}$$

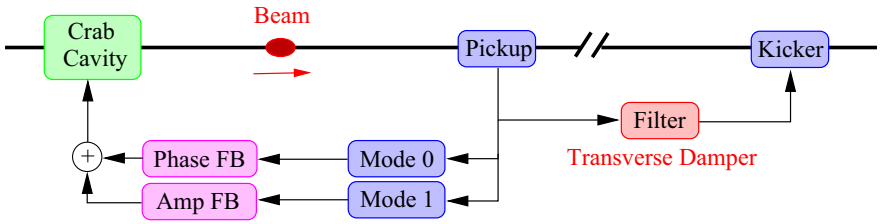

FIG. 6. Block diagram including damper and proposed feedback.

where σ_ϕ is the rms bunch length and $h_n = E[\sin(2\pi\nu_b n)]$ is the impulse response of the beam transfer function $H_{BTF}(z)$. Therefore,

$$E[\tilde{\boldsymbol{x}}_n] = \sqrt{\beta_{cc}}\frac{eV_o}{E_b}e^{-\frac{\sigma_\phi^2}{2}}\sum_{k=0}^{n} h_{n-k}\boldsymbol{\Delta\phi}_k = \sqrt{\beta_{cc}}\frac{eV_o}{E_b}e^{-\frac{\sigma_\phi^2}{2}} h_n * \boldsymbol{\Delta\phi}_n, \tag{10}$$

where the symbol $*$ denotes the convolution operator. The mean displacement caused by a crab cavity phase modulation is thus the convolution of the phase noise sequence with the impulse response of the beam transfer function, which gives the dependence on transverse tune distribution. The scaling by $e^{-\frac{\sigma_\phi^2}{2}}$ provides the dependence on the longitudinal distribution.

The variable $\tilde{\boldsymbol{x}}$ is normalized. To have physical units (meters), we must multiply by $\sqrt{\beta_p}$, where β_p is the β function at the pickup to evaluate the actual measured position shift $\tilde{X}_n$:

$$E[\tilde{\boldsymbol{X}}_n] = \sqrt{\beta_p\beta_{cc}}\frac{eV_o}{E_b}e^{-\frac{\sigma_\phi^2}{2}} h_n * \boldsymbol{\Delta\phi}_n. \tag{11}$$

The proposed feedback is shown in Fig. 7. It uses one pickup and N_{cc} crab cavities as kickers ($N_{cc} = 4$ for HL-LHC per beam and per plane). The feedback response is proportional to the pickup measurement (factor G_0), with a 90° phase shift (for positive frequencies around the beam response, −90° for negative frequencies), as shown in Fig. 7. The filter (impulse response g_n) also includes the appropriate phase shift to achieve a total phase advance of $\pi/2$ between the pickup measurement and the kick of each crab cavity, including the pickup to cavity betatron phase advance and the phase shift caused by the processing latency. The LHC and SPS transverse dampers use the same technique [28].

With $\boldsymbol{\Delta\phi}_n$ the sum of the phase noise of the N_{cc} cavities, from Fig. 7 and Eq. (11), we have

$$\boldsymbol{\Delta\phi}'_n = \boldsymbol{\Delta\phi}_n - g_n * \left(N_{cc}\sqrt{\beta_p\beta_{cc}}\frac{eV_0}{E_b}e^{-\frac{\sigma_\phi^2}{2}} h_n * \boldsymbol{\Delta\phi}'_n\right). \tag{12}$$

The overall loop gain is thus multiplied by the number of cavities used as kickers, as expected, since we apply the same correction to all cavities. The feedback loop includes the beam transfer function. With the feedback active, the phase noise $\boldsymbol{\Delta\phi}_n$ is modified resulting in the *effective* phase noise $\boldsymbol{\Delta\phi}'_n$, with a PSD varying within the tunespread. This *effective* phase noise is the one sensed by the beam.

When a random process $\boldsymbol{\Delta\phi}'_n$ is generated by filtering another random process $\boldsymbol{\Delta\phi}_n$ with a transfer function $K(e^{j2\pi\nu})$, its PSD is the product of the PSD of $\boldsymbol{\Delta\phi}_n$ and the squared modulus of $K(e^{j2\pi\nu})$. In our case, the transfer function $K(e^{j2\pi\nu})$ is the closed-loop response of the feedback loop shown in Fig. 7. It is thus possible to calculate the noise PSD experienced by the particles:

$$S_{\Delta\phi'}[(k+\nu_b)f_{\text{rev}}] = \frac{S_{\Delta\phi}[(k+\nu_b)f_{\text{rev}}]}{\left|1 + jG_0N_{cc}\sqrt{\beta_p\beta_{cc}}\frac{eV_0}{E_b}e^{-\frac{\sigma_\phi^2}{2}}H_{\text{BTF}}(e^{j2\pi\nu_b})\right|^2}, \tag{13}$$

where $H_{\text{BTF}}(e^{j2\pi\nu_b})$ is the beam transfer function $H_{\text{BTF}}(z)$ evaluated on the unit circle at tune ν_b.

This *effective* phase noise spectrum varies significantly within the tune spread. It will therefore result in different

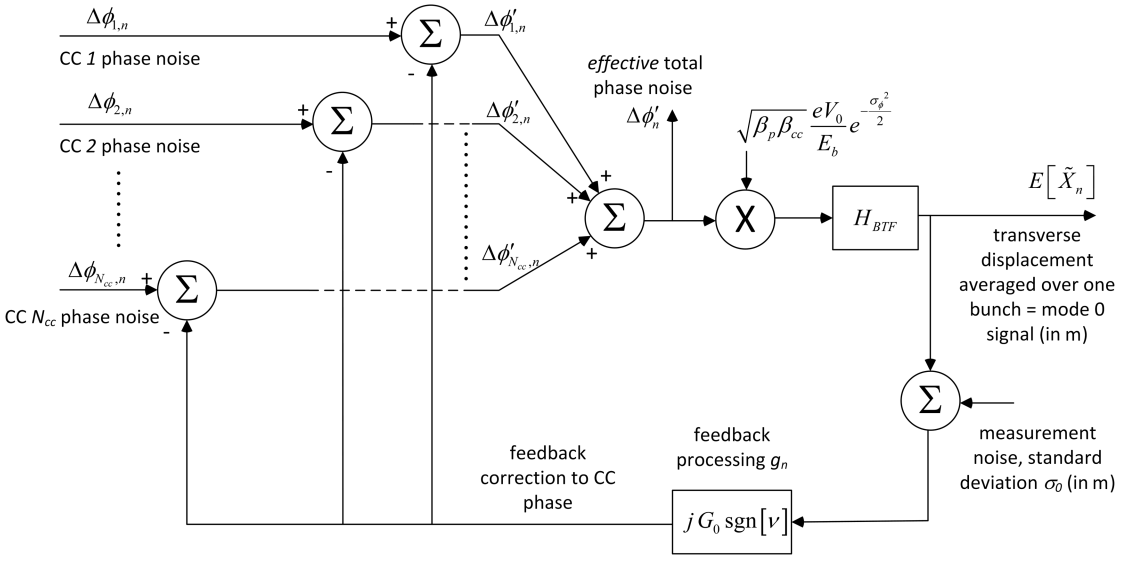

FIG. 7. Crab cavity phase feedback (mode 0).

oscillation growth for particles at different ν_b: the noise spectrum is reduced significantly for tunes corresponding to many particles (typically the bunch core) where H_{BTF} is large but is not modified for weakly populated tunes (bunch tails). The tune-dependent reduction factor is

$$R_\phi(\nu_b) = \frac{S_{\Delta\phi'}[(k+\nu_b)f_{\mathrm{rev}}]}{S_{\Delta\phi}[(k+\nu_b)f_{\mathrm{rev}}]} = \frac{1}{\left|1 + jG_0N_{cc}\sqrt{\beta_p\beta_{cc}}\frac{eV_0}{E_b}e^{-\frac{\sigma_\phi^2}{2}}H_{\mathrm{BTF}}(e^{j2\pi\nu_b})\right|^2}. \tag{14}$$

As shown in Sec. VII C of [9] for the case of a transverse damper, we now need to integrate over the bunch tune distribution to get the reduction in emittance growth. We get

$$\begin{aligned}\overline{R_\phi} &= \int_{-\infty}^{\infty} \frac{\rho(\nu_b)}{\left|1 + jG_0N_{cc}\sqrt{\beta_p\beta_{cc}}\frac{eV_0}{E_b}e^{-\frac{\sigma_\phi^2}{2}}H_{\mathrm{BTF}}(e^{j2\pi\nu_b})\right|^2}d\nu_b \\ &= \frac{1}{\pi}\int_{-\infty}^{\infty} \frac{g(u)}{\left[1 + \frac{G_0N_{cc}\sqrt{\beta_p\beta_{cc}}eV_0e^{-\frac{\sigma_\phi^2}{2}}}{4\pi\sigma_{\nu_b}E_b}g(u)\right]^2 + \left[\frac{G_0N_{cc}\sqrt{\beta_p\beta_{cc}}eV_0e^{-\frac{\sigma_\phi^2}{2}}}{4\pi\sigma_{\nu_b}E_b}f(u)\right]^2}du \\ &= \frac{1}{\pi}\int_{-\infty}^{\infty} \frac{g(u)}{[1+\alpha_0 g(u)]^2 + [\alpha_0 f(u)]^2}du, \end{aligned} \tag{15}$$

where

$$\begin{aligned} u &= \frac{\overline{\nu_b} - \nu_b}{\sigma_{\nu_b}} \\ g(u) &= \pi\sigma_{\nu_b}\rho(\overline{\nu_b} - u\sigma_{\nu_b}) \\ f(u) &= \sigma_{\nu_b}\ \mathrm{P.V.}\int_{-\infty}^{\infty}\frac{\rho(\nu_b)}{(\nu_b - \overline{\nu_b} + u\sigma_{\nu_b})}d\nu_b \\ H_{\mathrm{BTF}}(e^{j2\pi\nu_b}) &= \frac{1}{4\pi j\sigma_{\nu_b}}g(u) + \frac{1}{4\pi\sigma_{\nu_b}}f(u) \\ \alpha_0 &= \frac{G_0N_{cc}\sqrt{\beta_p\beta_{cc}}eV_0e^{-\frac{\sigma_\phi^2}{2}}}{4\pi\sigma_{\nu_b}E_b} \end{aligned} \tag{16}$$

and $\overline{\nu_b}$ is the mean betatron tune. The functions $g(u)$, $f(u)$ are provided for various distributions in [29].

For a given tune distribution, the feedback action on the full bunch emittance growth depends only on α_0. If the feedback phase is optimally adjusted, the resulting damping time τ_0 will be twice the revolution period divided by the overall loop gain [30]. As a result and using Fig. 7,

$$\tau_0 = \frac{2T_{\mathrm{rev}}}{G_0N_{cc}\sqrt{\beta_p\beta_{cc}}\frac{eV_0}{E_b}e^{-\frac{\sigma_\phi^2}{2}}} = \frac{1}{\alpha_0}\frac{T_{\mathrm{rev}}}{2\pi\sigma_{\nu_b}}. \tag{17}$$

The feedback will mitigate the noise if the damping time τ_0 is smaller than the decoherence time $\tau_d = T_{\mathrm{rev}}/(2\pi\sigma_{\nu_b})$. Actually, α_0 is exactly equal to the ratio of these time constants.

It is possible to calculate the correction factor $\overline{R_\phi}$ as a function of α_0 for various distributions, including $\rho_{\mathrm{sim}}(\nu_b)$ defined in Sec. II, as shown in Fig. 8. All the curves asymptotically approach $1/\alpha_0^2$ when the damping time becomes much smaller than the betatron decoherence time ($\alpha_0 \gg 1$). This approximation was derived in [31,32] for dipole kicks.

Not surprisingly, this is equivalent to the reduction achieved by the transverse damper for very short bunches in [9]. However, the phase feedback will provide the same reduction, independent of bunch length.

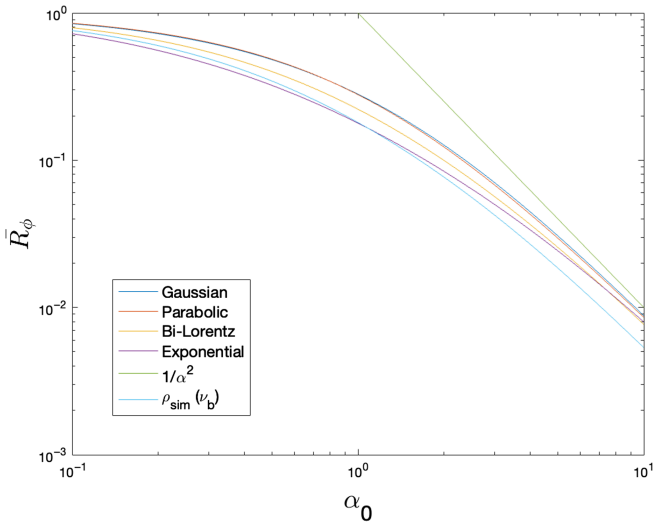

FIG. 8. Emittance growth reduction factor as a function of α_0 and tune distribution.

B. Emittance growth reduction with mode 1 feedback

The corresponding derivation for mode 1 is presented in Appendix B. The achieved amplitude noise power reduction at betatron tune ν_b, when feeding back on N_{cc} cavities, is given by

$$R_A(\nu_b) = \frac{1}{\left|1 + jG_1 N_{cc} \frac{2\pi\sqrt{\beta_p \beta_{cc}}}{\lambda} \frac{eV_0}{E_b} e^{-\frac{\sigma_\phi^2}{2}} [H_{\mathrm{BTF}}(e^{j2\pi[\nu_b + \overline{\nu_s}]}) + H_{\mathrm{BTF}}(e^{j2\pi[\nu_b - \overline{\nu_s}]})]\right|^2}, \tag{18}$$

where λ is the rf wavelength.

Taking the ensemble average over the betatron tune distribution as done for the phase noise, and using the same notation for the beam transfer function, we get

$$\overline{R_A} = \frac{1}{\pi} \int_{-\infty}^{\infty} \frac{g(u)}{\left[1 + \alpha_1 \frac{g(u + \frac{\overline{\nu_s}}{\sigma_{\nu_b}}) + g(u - \frac{\overline{\nu_s}}{\sigma_{\nu_b}})}{2}\right]^2 + \left[\alpha_1 \frac{f(u + \frac{\overline{\nu_s}}{\sigma_{\nu_b}}) + f(u - \frac{\overline{\nu_s}}{\sigma_{\nu_b}})}{2}\right]^2} du, \tag{19}$$

where

$$\alpha_1 = \frac{G_1 N_{cc} \sqrt{\beta_p \beta_{cc}} e V_0 e^{-\frac{\sigma_\phi^2}{2}}}{\lambda \sigma_{\nu_b} E_b}. \tag{20}$$

The correction factor $\overline{R_A}$ is shown in Fig. 9 as a function of α_1 for the exponential and the $\rho_{\mathrm{sim}}(\nu_b)$ tune distributions, for $\overline{\nu_s} = 0.002$. The synchrotron tune has a small negative impact on the achieved reduction.

The resulting damping time is given by

$$\tau_1 = \frac{2T_{\mathrm{rev}}\lambda}{4\pi G_1 N_{cc} \sqrt{\beta_p \beta_{cc}} \frac{eV_0}{E_b} e^{-\frac{\sigma_\phi^2}{2}}} = \frac{1}{\alpha_1} \frac{T_{\mathrm{rev}}}{2\pi\sigma_{\nu_b}}. \tag{21}$$

The amplitude feedback will mitigate the noise for large values of α_1, that is, if the damping time τ_1 is smaller than the decoherence time $T_{\mathrm{rev}}/(2\pi\sigma_{\nu_b})$.

C. Measurement noise effects

The crab cavity feedback appears very promising for rf noise mitigation. As it relies on beam-based measurements (bunch displacement and tilt), we anticipate that its performance will be determined by the precision of these measurements. In the present section, we derive formulas for the effects of such errors.

We consider the phase feedback first. As seen in Fig. 7, the measurement noise (error in the measurement of the bunch transverse displacement) is added to the rf phase noise of *each* cavity after scaling by gain G_0. It is therefore added to the phase noise sum $\boldsymbol{\Delta\phi}'_n$ with gain $N_{cc}G_0$. Merging Eqs. (1), (4), (6), and (15), the emittance growth rate will be

$$\begin{aligned}
\frac{d\epsilon_n}{dt} &= 2\gamma\beta_{cc} \left(\frac{eV_o f_{\mathrm{rev}}}{2E_b}\right)^2 C_{\Delta\phi}(\sigma_\phi) \overline{R_\phi} \left[N_{cc} S_{\Delta\phi,\mathrm{eff}} + {N_{cc}}^2 {G_0}^2 \frac{{\sigma_0}^2}{f_{\mathrm{rev}}}\right] \\
&= 2N_{cc}\gamma\beta_{cc} \left(\frac{eV_o f_{\mathrm{rev}}}{2E_b}\right)^2 C_{\Delta\phi}(\sigma_\phi) \frac{1}{f_{\mathrm{rev}}} \overline{R_\phi} [\sigma_{\Delta\phi}^2 + N_{cc} G_0^2 \sigma_0^2] \\
&= 2N_{cc}\gamma\beta_{cc} \left(\frac{\mathrm{e}V_o f_{\mathrm{rev}}}{2E_b}\right)^2 C_{\Delta\phi}(\sigma_\phi) \frac{1}{f_{\mathrm{rev}}} \overline{R_0} \sigma_{\Delta\phi}^2 \\
\overline{R_0} &= \overline{R_\phi} \left[1 + N_{cc} G_0^2 \frac{\sigma_0^2}{\sigma_{\Delta\phi}^2}\right],
\end{aligned} \tag{22}$$

where we are assuming N_{cc} cavities with effective PSD $S_{\Delta\phi,\mathrm{eff}}$ per cavity, independent rf phase noise, and white measurement noise of standard deviation σ_0.

We can similarly quantify the effect of the bunch tilt pickup measurement imprecision on the amplitude feedback. Referring to Fig. 17, we see that this noise is added to the cavity amplitude noise of each cavity, with a scaling by G_1. Merging Eqs. (2), (5), (7), and (19), the resulting emittance growth rate will be

$$\frac{d\epsilon_n}{dt} = 4\gamma\beta_{cc}\left(\frac{eV_o f_{\text{rev}}}{2E_b}\right)^2 C_{\Delta A}(\sigma_\phi)\overline{R_A}\left[N_{cc}S_{\Delta A,\text{eff}} + {N_{cc}}^2{G_1}^2\frac{{\sigma_1}^2}{f_{\text{rev}}}\right]$$
$$= 4N_{cc}\gamma\beta_{cc}\left(\frac{eV_o f_{\text{rev}}}{2E_b}\right)^2 C_{\Delta A}(\sigma_\phi)\frac{1}{f_{\text{rev}}}\overline{R_A}[\sigma_{\Delta A}^2 + N_{cc}G_1^2\sigma_1^2]$$
$$= 4N_{cc}\gamma\beta_{cc}\left(\frac{eV_o f_{\text{rev}}}{2E_b}\right)^2 C_{\Delta A}(\sigma_\phi)\frac{1}{f_{\text{rev}}}\overline{R_1}\sigma_{\Delta A}^2$$
$$\overline{R_1} = \overline{R_A}\left[1 + N_{cc}G_1^2\frac{\sigma_1^2}{\sigma_{\Delta A}^2}\right]. \tag{23}$$

In the above equations, the effect of the rf noise scales linearly with the number of cavities (addition in power) as their noise processes are assumed uncorrelated. However, identical measurement noise samples are injected in each cavity feedback, resulting in a quadratic scaling factor.

As expected, the emittance growth rate reduction ($\overline{R_0}$, $\overline{R_1}$) is less effective with increasing measurement noise. The crab cavity noise dominates the emittance growth for low feedback gains and that makes the system beneficial ($\overline{R_\phi}$, $\overline{R_A}$ decrease with increasing G_0, G_1 as shown in Figs. 8 and 9), whereas the measurement noise dominates for very high feedback gains (its contribution is scaled by G_0^2, G_1^2) resulting in detrimental effects. Therefore, in the presence of measurement noise, we anticipate a limitation on the feedback performance and the existence of an optimal gain beyond which the feedback actually becomes detrimental.

D. Optimal β_p value

The crab cavities must be placed at a high β location to achieve the required crabbing angle with the smallest possible voltage.

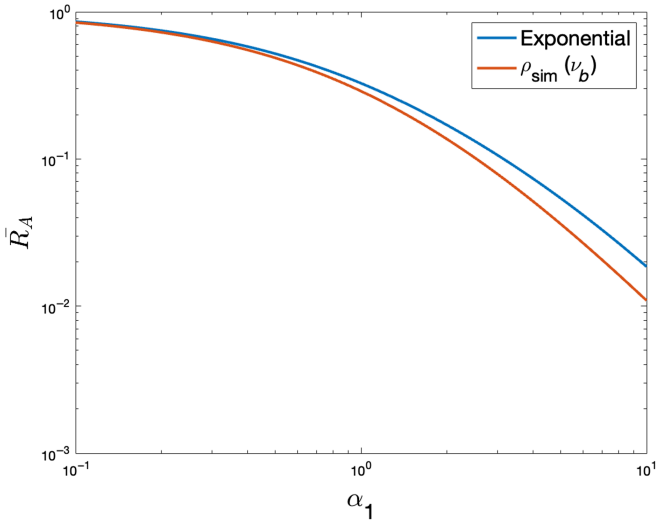

FIG. 9. Emittance growth reduction factor as a function of α_1 and tune distribution.

The ratio of the measured deviation at the pickup and the phase noise at the crab cavity is proportional to the square root of the product of the β function values at those two points (Fig. 7). Note that for a higher β_p, lower G_0 and G_1 are needed to maintain the same emittance growth rate reduction [Eqs. (16) and (20)]. Consequently, a high β_p also reduces the effect of measurement noise, as expected.

The pickup is placed at a high β position in the planned layout, very close to the crab cavities. In this work, we use $\beta_p = 2000$ m at the pickup. The exact value will depend on the final optics. This is a conservative estimate.

E. Maximum loop gain as a function of loop delay

The feedback systems shown in Figs. 7 and 17 include no delay from the pickup measurement to the correcting kick (crab cavity phase or amplitude). In the HL-LHC layout, the pickup will be located close to the crab cavity. However, time will be required for the signal processing, as well as for the appropriate filtering to apply an exact 90° phase shift [28]. As a result, the overall loop delay will be at least a few turns, which will limit the maximum possible loop gain. We will now relate the maximum loop gain to the loop delay. We consider the phase feedback first.

With the addition of a delay τ_L in the feedback processing (filter impulse response g_n) in Fig. 7, and after adjusting the phase to be 90° at the mean betatron tune $\overline{\nu}_b$, the open loop response $G_{ol}(\nu)$ becomes

$$G_{ol}(\nu) = j\,4\pi\sigma_{\nu_b}\alpha_0 e^{-j2\pi\tau_L f_{\text{rev}}(\nu-\bar{\nu}_b)}H_{\text{BTF}}(e^{j2\pi\nu}). \tag{24}$$

Using the normalized expression for H_{BTF} [Eq. (16)], we can express the open loop response as a function of variable u

$$H_{ol}(u) = \alpha_0 e^{j2\pi\tau_L\sigma_{\nu_b}f_{\text{rev}}u}[g(u) + j\,f\,(u)]. \tag{25}$$

Now with the decoherence time $\tau_d = T_{\text{rev}}/(2\pi\sigma_{\nu_b})$, we have

$$H_{ol}(u) = \alpha_0 e^{j\frac{\tau_L}{\tau_d}u}[g(u) + j\,f\,(u)]. \tag{26}$$

The open loop response only depends on the ratio of the loop delay over decoherence time and on the normalized beam transfer function. A classic method to design a robust feedback system is to impose a sufficient *gain margin*, that is a factor by which the open loop gain must be increased before causing the system to go unstable. As instability arises when the phase of the open loop response is 180°, this classic design method requires that the amplitude of H_{ol} be below 0.32 linear at the frequency where its phase is 180°. A 10 dB gain increase (3.16 linear) is then required to drive the system unstable. For the crab cavity feedback to be efficient, its response time must be significantly faster than the decoherence time. Its closed loop bandwidth will therefore be much larger than the tune spread. As a consequence, the open loop will reach amplitude 0.32 at a frequency well outside the tune spectrum. In this range, $H_{\mathrm{BTF}}(u) \propto [f(u) + j\,g(u)]$ is almost purely real since $g(u) \approx 0$. It is actually exactly real for parabolic and elliptical tune distributions [29]. Now setting $g(u) = 0$ in Eq. (26), we conclude that the open loop response phase reaches 180° when the loop delay has added 90° of phase shift, that is, at $u_\pi = (\pi\tau_d)/(2\tau_L)$. Finally, imposing that the amplitude of the open loop response is 0.32 at u_π, we obtain the *optimal* loop gain

$$\alpha_{0,\mathrm{opt}} = \frac{0.32}{|f(\frac{\pi}{2}\frac{\tau_d}{\tau_L})|}. \tag{27}$$

Far outside the tune distribution ($|u| \gg 1$), the $f(u)$ function can be approximated by $f(u) \approx 1/u$. With this simplification, we obtain a simple expression for the optimal loop gain

$$\alpha_{0,\mathrm{opt}} = 0.32\frac{\pi}{2}\frac{\tau_d}{\tau_L} \approx \frac{1}{2}\frac{\tau_d}{\tau_L}. \tag{28}$$

The same formula can be derived from Fig. 17 for the optimal amplitude feedback gain $\alpha_{1,\mathrm{opt}}$.

It is worth noting that one can operate the feedback systems with a lower loop gain, as long as it is sufficient to reduce the rf noise effects within specifications. However, operation with gain higher than the above figure will result in a *ringing* response first and then lead to loop instability when $\alpha \approx 3.16\alpha_{\mathrm{opt}}$.

F. Interaction with the transverse damper

It should be noted that the reduction $\overline{R_\phi}$ due to crab cavity phase feedback and $\overline{R_d}$ due to the transverse damper [Eq. (3)] are *not* multiplicative. Comparing Fig. 5 of [9] with Fig. 7 above, we see that the two systems implement parallel feedback loops. They both use a measurement of the dipole motion to generate a transverse damping kick. The difference rests in the kicker only. The transverse damper uses a 20 MHz bandwidth kicker (bunch-by-bunch operation with 25 ns bunch spacing [33]) while the crab cavity phase feedback generates transverse momentum kicks via phase modulation of the crab cavity rf. Their combined effect will therefore not be *multiplicative* in reduction factor, but rather will be *additive* in feedback loop gain: the transverse damper α [Eq. (28) in [9]] will be added to the noise feedback α_0. The HL-LHC crab cavity feedback damping time will be around ten turns (Sec. VIII A), while the transverse damper has 50 turns damping time in stable beams [21]. It will therefore provide only marginal improvement to the reduction of the crab cavity noise effect in the presence of the phase feedback.

G. Crab cavity rf noise feedback bandwidth

The HL-LHC beam consists of batches of 25 ns spaced bunches with a batch duration of up to 7.2 μs. As shown in Sec. V, the strong rf feedback results in a 136 kHz regulation bandwidth, which matches the noise PSD bandwidth (Fig. 5). The crab cavity feedback will only modulate the crab cavity voltage phase and amplitude within the 136 kHz bandwidth and will sufficiently compensate for the crab cavity rf noise.

Note that the cavity Q_L is 500,000, resulting in a single-sided bandwidth of 400 Hz. It would thus take a lot of rf power to generate large variations of the field at 136 kHz. However, the modulation is only required to compensate for the very low levels of rf noise.

VII. CRAB CAVITY RF NOISE FEEDBACK SIMULATIONS

Simulations were performed to validate the above analytical derivations and confirm the possible performance improvement with such a feedback system. The simulations used the HEADTAIL code, a software package developed at CERN for the simulation of multiparticle beam dynamics with collective effects [34,35]. The code includes various beam and machine parameters and computes the evolution of individual particles within a bunch over an adjustable number of turns. It includes betatron and synchrotron motion for each particle, coupling in the transverse plane, chromaticity, and momentum spread in all three axes. This software package was also used to validate the theoretical relationship between crab cavity rf noise and transverse emittance growth presented in [9].

Simulations in [9] are of a single-beam model, whereas [10] includes beam-beam effects. There is very good agreement between them. Therefore, a single-beam model is used in the simulations presented in this work. The nonlinear transverse mechanism provided by the beam-beam interaction is modeled in the single-beam simulations through increased octupole action.

As the noise spectrum extends to 136 kHz (Fig. 5), the turn-by-turn samples will be uncorrelated ($f_{\mathrm{rev}} = 11.245$ kHz). In the simulations, the noise is white and is applied once per turn. Its spectrum is therefore flat

from $-f_{\mathrm{rev}}/2$ to $f_{\mathrm{rev}}/2$ with rms values $\sigma_{\Delta\phi}$ and $\sigma_{\Delta A}$. The simulations are conducted with one bunch only and one crab cavity ($N_{cc} = 1$). All other parameters are as in the HL-LHC.

The simulated crab cavity feedback input extracts the bunch mean displacement $E[\tilde{X}]$ (mode 0 motion in meters) and the bunch tilt $\frac{E[\tilde{X}z]}{\sigma_z{}^2}$ (mode 1 motion in radians). Appendix B presents the bunch tilt measurement in more detail. These two signals are used as the error input for the phase and amplitude feedback branches, respectively. White noise is added to the estimated mode 0 and mode 1 motion to mimic measurement noise, which leads to noise in the correction kicks, decreasing the effectiveness of the feedback (Sec. VI C).

As shown in Sec. V, the LLRF regulation bandwidth is limited to 136 kHz, leading to a response time of 1.17 μs, much smaller than the revolution period (89 μs). Therefore, we can assume that in the simulations, the crab cavity voltage is modulated by the feedback turn by turn.

The amplitude and phase feedback systems were first examined separately, by only using one type of noise kick and feedback at a time, and without measurement noise (Figs. 10 and 11). The vertical axis represents the emittance growth reduction factor. The horizontal axis is α_0 and α_1, respectively (proportional to the feedback damping rate). The transverse damper is off for these simulations. A significant reduction in emittance growth rate is achieved as the feedback damping rates are increased. The effect is reproducible for a range of crab cavity noise levels.

Both feedback systems were combined to act on both types of noise simultaneously. The resulting emittance growth rate is the sum of the growth rate found for each feedback separately. As expected, the two feedback systems behave independently, without influencing each other.

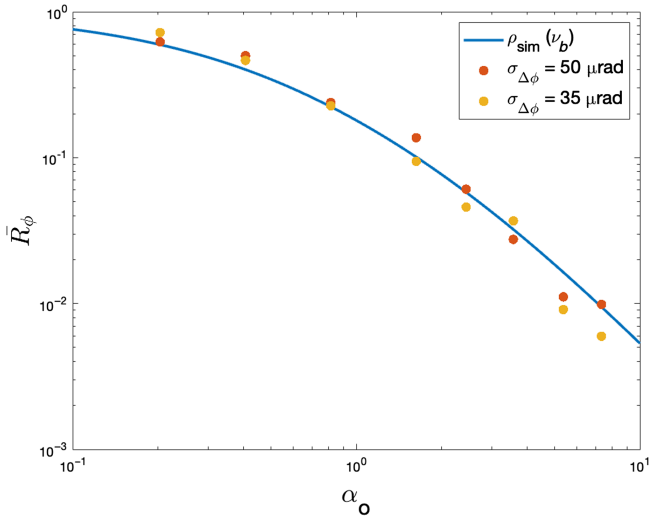

FIG. 10. Emittance growth reduction factor from phase feedback acting on phase noise. The solid line is the analytical formula [Equation (15)]. The dots are simulation results with one cavity ($N_{cc} = 1$).

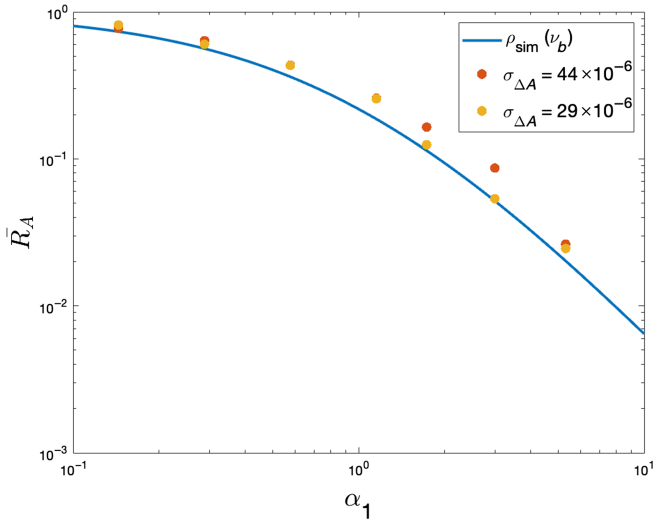

FIG. 11. Emittance growth reduction factor from amplitude feedback acting on amplitude noise. The solid line is the analytical formula [Equation (19)]. The dots are simulation results with one cavity ($N_{cc} = 1$).

We next introduced measurement noise in the simulation, in either mode 0 (Fig. 12) or mode 1 (Fig. 13). As expected from Eqs. (22) and (23), the emittance growth rate reduction is less effective with increasing measurement noise. The crab cavity noise dominates the emittance growth for low feedback gains, whereas the measurement noise dominates for very high feedback gains.

In our simulations, the phase advance is set to $\pi/2$. Simulations were performed with various other phase advance values. The effectiveness of the crab cavity

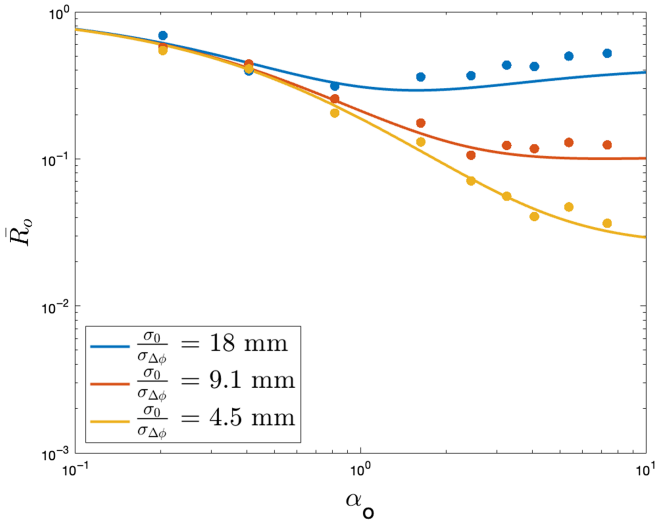

FIG. 12. Emittance growth reduction factor with varying mode 0 measurement error to phase noise ratios. $N_{cc} = 1$.

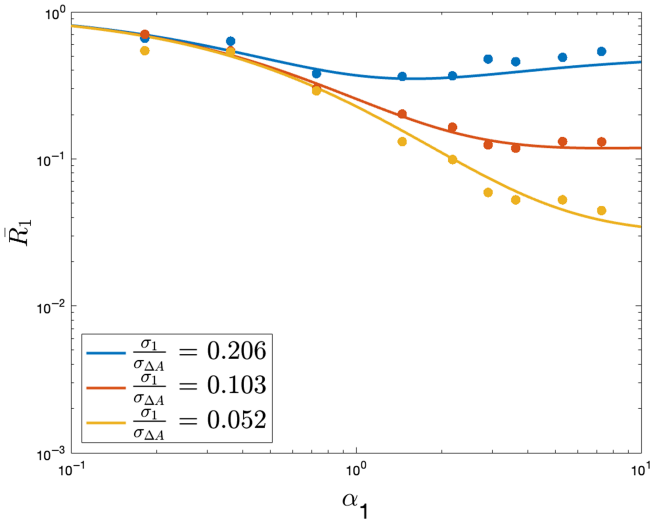

FIG. 13. Emittance growth reduction factor with varying mode 1 measurement error to amplitude noise ratios. $N_{cc} = 1$.

feedback was significantly reduced as a result, a classic behavior common to all transverse feedback systems.

Further studies were performed to evaluate the feedback system's interaction with the LHC transverse damper [36]. The two systems are complementary and no issues were observed when they were both active.

These extensive simulations validate the analytical expressions derived in Sec. VI and confirm that the most critical parameter for the crab cavity rf noise feedback system is the measurement noise.

VIII. CRAB CAVITY FEEDBACK DESIGN: LOOP GAINS AND MEASUREMENT NOISE THRESHOLD

It is clear from Figs. 12 and 13 that the proposed feedback system has the potential to significantly reduce the emittance growth rate due to crab cavity rf noise in the HL-LHC. The performance of this system is dependent on the measurement noise level and the loop gains α_0 and α_1. Using the theory presented in this work, we can now design the crab cavity feedback to achieve the required reduction.

A. Optimal gain

With the HL-LHC parameters listed in Table I, we compute a decoherence time $\tau_d = 4.72$ ms. From past experience with the SPS and LHC transverse dampers, we anticipate a three to five turns loop delay [28]. Using Eq. (28) and the more conservative five turns ($\tau_L = 0.445$ ms), we obtain feedback gains $\alpha_{0,\mathrm{opt}} = \alpha_{1,\mathrm{opt}} = \frac{1}{2}\frac{\tau_d}{\tau_L} = 5.3$, resulting in a feedback damping time of 0.89 ms (ten turns). See Eqs. (17) and (21).

B. Measurement noise thresholds

To achieve the 1% integrated luminosity loss target mentioned in Sec. IV B, the maximum noise contribution to emittance growth rate is just 2%/hour. The estimated HL-LHC phase and amplitude noise spectra presented in Sec. V (Fig. 5) will result in 23.7%/h emittance growth due to phase noise and 9.0%/h due to amplitude noise, without contribution from the transverse damper (Sec. V).

The HL-LHC transverse damper will provide phase noise reduction, insufficient to achieve the emittance growth requirement ($\overline{R_d} = 0.32$, Sec. IV D). In addition, the contributions from the damper and the noise feedback are not multiplicative in reduction factor (Sec. VI F). Therefore, the damper will only provide marginal additional reduction. In this work, we use a conservative approach and design the noise feedback assuming *no reduction from the damper.*

Allowing for 1%/hour for each noise source, we must therefore reduce the phase noise effect by a factor of 25 ($\overline{R_0} = 0.04$) and the amplitude noise by a factor of 10 ($\overline{R_1} = 0.1$). Note that the phase and amplitude noise contributions could be partitioned differently depending on the achieved mode 0 and mode 1 pickup precision. For example, if the contributions were 1.45% and 0.55%, respectively, both reduction factors would have to be about 16.4.

These reduction factors can be achieved with various combinations of measurement noise to rf noise ratios and feedback gains [Eqs. (22) and (23)], as seen in Figs. 14 and 15. Various combinations of noise ratios and gains satisfy the requirements, as long as we stay to the left of the $\alpha = 5.3$ line and below the emittance growth rate reduction goal. The limiting noise ratio is given by the curve passing through the intersection of these two lines.

For $\alpha = 5.3$, $\overline{R_\phi} = 0.0255$, and $\overline{R_A} = 0.043$. Then, using Eqs. (22) and (23), $N_{cc} = 4$, an exponential distribution,

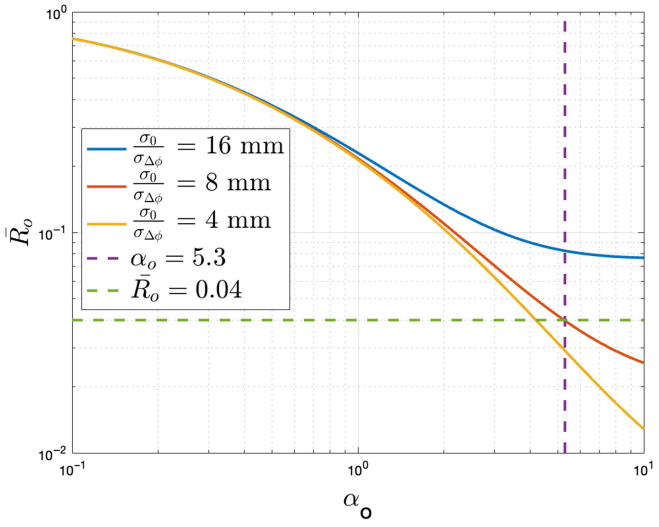

FIG. 14. Emittance growth reduction factor with varying mode 0 measurement error to phase noise ratios. HL-LHC case ($N_{cc} = 4$).

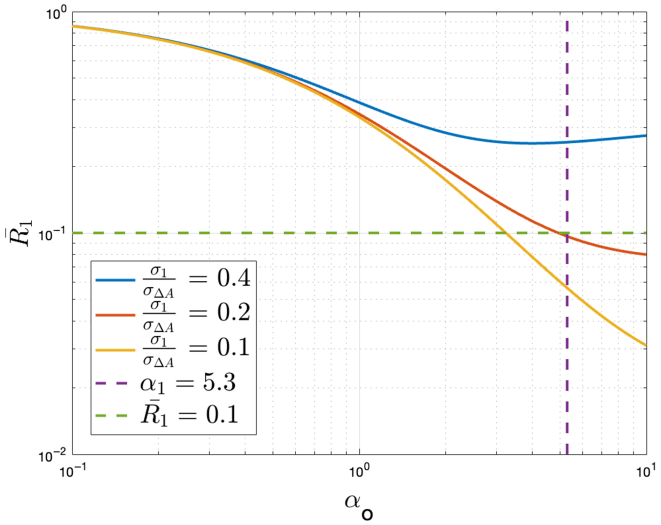

FIG. 15. Emittance growth reduction factor with varying mode 1 measurement error to amplitude noise ratios. HL-LHC case ($N_{cc} = 4$).

and the reduction factors of $\overline{R_0} = 0.04$ and $\overline{R_1} = 0.1$, we get that

$$\frac{\sigma_0}{\sigma_{\Delta\phi}} < 8.1 \text{ mm},$$
$$\frac{\sigma_1}{\sigma_{\Delta A}} < 0.21.$$

In Sec. V, we determined that the effective noise spectrum would be at least: $S_{\Delta\phi,\text{eff}}(f) = 0.141\ (\mu\text{rad})^2/\text{Hz}$ and $S_{\Delta A,\text{eff}}(f) = 0.141 \times 10^{-12}$ 1/Hz. As a result, $\sigma_{\Delta\phi} = 40$ μrad and $\sigma_{\Delta A} = 40 \times 10^{-6}$. The measurement noise thresholds are thus $\sigma_0 < 320$ nm and $\sigma_1 < 8.3$ μrad. These are bunch-by-bunch measurement levels and are a function of the β function at the pickup ($\beta_p = 2000$ m).

The above measurement noise thresholds ($\sigma_0 < 320$ nm and $\sigma_1 < 8.3$ μrad) require extremely high precision measurements. Fortunately, the closed loop bandwidth of the crab cavity with LLRF field regulation will only extend to 136 kHz (Sec. V). As a result, the noise bandwidth will also be limited to 136 kHz. In addition, the bunches are spaced every 25 ns and the measurement noise is uncorrelated from bunch to bunch. Therefore, there is white measurement noise extending to 20 MHz (half the sampling frequency). Filtering the data with a low-pass filter matching the signal spectrum will scale the measurement noise power by a factor of 136 kHz/20 MHz = 0.0068. The noise standard deviation would be scaled by 0.0825 ($= \sqrt{0.0068}$), a factor of about 12 (linear) improvement in signal-to-noise ratio. This increases the actual single bunch resolution threshold to 3.9 μm rms and 100 μrad rms. This is a tight, but achievable specification. For mode 0, for example, the LHC transverse damper had a resolution of about 1 to 1.4 μm rms during runs 1 and 2 and could be up to a factor of 6 lower in run 3 [37]. Studies are ongoing to determine the pickup type and associated rf processing chain to achieve the above mode 0 and 1 resolution.

IX. CONCLUSIONS

This work presents the estimated transverse emittance growth rate due to crab cavity rf noise in the HL-LHC. The emittance growth rate will be very high if the LLRF technology mirrors the present LHC accelerating cavities. Ambitious LLRF improvements will be implemented to reduce the noise spectra by at least 10 dB at 3 kHz and above, compared to the LHC accelerating cavity noise spectrum. These improvements would achieve a 32.7%/hour emittance growth rate, still far from the 2%/hour target.

A mitigation is presented, consisting of a dedicated feedback system acting via the crab cavities to further reduce the effect of rf noise. The measurement part of this feedback system could work in tandem with the bunch-by-bunch transverse damper. After processing, it would modulate the crab cavity phase and amplitude, which is used as a kicker, thereby correcting for both phase and amplitude noise. We presented analytical derivations on the performance and limitations of this novel crab cavity rf noise feedback system. We also performed extensive simulations to validate our theoretical formalism. The analytical expressions and simulations show that the proposed system has the potential to significantly reduce the transverse emittance growth due to crab cavity rf noise. Our studies also show that the most critical parameter for this novel feedback system is the pickup measurement noise. This analytical work is applicable to other accelerators employing crab cavities.

We have presented a design for the crab cavity feedback that fulfills the HL-LHC requirements. This design includes numbers of mode 0 (dipole) and mode 1 (tilt) transverse motions. Studies are ongoing on the selection of a pickup design fulfilling these measurement noise specifications.

ACKNOWLEDGMENTS

We thank E. Metral, R. Tomas, N. Mounet, X. Buffat, L. Giacomel (CERN) for their explanations on the HL-LHC stable beams parameters and for hosting presentations on this work. We are grateful to D. Valuch and G. Kotzian for discussions and technical information on the front end of the proposed feedback system and on the processing of the SPS transverse feedback. We would also like to thank M. Krupa and T. Levens from the Beam Instrumentation group for their input on the proposed crab cavity feedback pickup. Machine development sessions were conducted in the SPS (2018, 2021, 2022) to collect transverse emittance growth measurements due to crab cavity rf phase and amplitude noise. In addition to the authors, the following people have

participated: N. Triantafyllou, F. Antoniou, H. Bartosik, P. X. Buffat, R. Calaga, Y. Papaphilippou, A. Wolski (Accelerator Physics), L. R. Carver, T. Levens (Beam Instrumentation), J. Egli, N. Stapley (LLRF and controls). The LHC crab cavity project is led by R. Calaga. We thank him for the support in developing a LLRF for this future system and for the effort in investigating emittance growth with the SPS crab cavity test stand. This work is supported by the U.S. Department of Energy, Office of Science, Office of High Energy Physics, under Award No. DE-SC-0019287. This research is also supported by the HL-LHC project.

APPENDIX A: $C_{\Delta\phi}(\sigma_\phi)$ FOR A PILLBOX DISTRIBUTION

The longitudinal distribution can vary significantly. In this section, the $C_{\Delta\phi}(\sigma_\phi)$ factors are computed for a two-dimensional pillbox distribution in longitudinal phase space ("water-bag" bunch [29]). This distribution is in many ways the exact opposite of a two-dimensional Gaussian shown in the main text: it is uniform and has well-defined and sharp edges. In this case, the peak amplitude of the synchrotron oscillation $\hat{\boldsymbol{\phi}}$ follows a triangular distribution with density function

$$f_{\hat{\phi}}(\hat{\phi}) = 2\hat{\phi}/\hat{\phi}_{\max}{}^2$$

for $\hat{\phi}$ in $[0, \hat{\phi}_{\max}]$.

Then, using this distribution in place of the Rayleigh distribution in Appendix A of [9],

$$C_{\Delta\phi}(\sigma_\phi) = J_0^2[\hat{\phi}_{\max}] + J_1^2[\hat{\phi}_{\max}] + 2\sum_{n=1}^{\infty}\left[J_{2n}^2[\hat{\phi}_{\max}] - \frac{4nJ_{2n}[\hat{\phi}_{\max}]J_{2n+1}[\hat{\phi}_{\max}]}{\hat{\phi}_{\max}} + J_{2n+1}^2[\hat{\phi}_{\max}]\right].$$

Figure 16 shows the factors for the Gaussian and pillbox cases as a function of the full width at half maximum (FWHM) of the longitudinal line density (FWHM $= 2\sqrt{2\log 2}\sigma_\phi$ for Gaussian and FWHM $= \sqrt{3}\hat{\phi}_{\max}$ for pillbox). The factors change only slightly between these two extreme distributions.

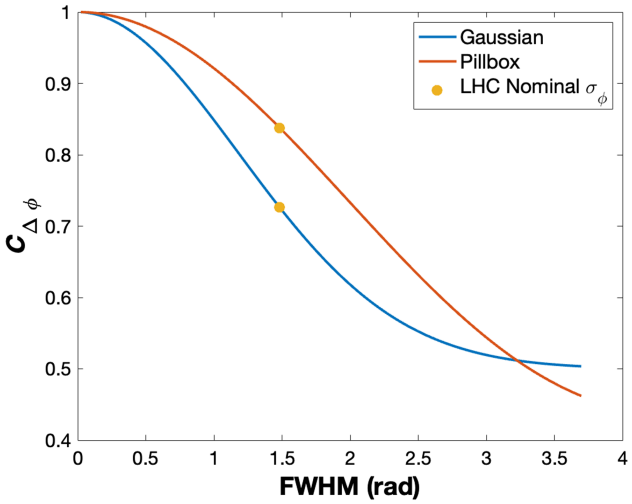

FIG. 16. Bunch length correction factors for two-dimensional Gaussian and pillbox distributions.

APPENDIX B: EMITTANCE GROWTH REDUCTION WITH MODE 1 FEEDBACK

Following the derivation presented in Eqs. (2) and (8) in [9], the momentum kicks from a single cavity (voltage V_0), caused by the amplitude noise sequence $\boldsymbol{\Delta A}_k$, result in the normalized position shift $\tilde{\boldsymbol{x}}_n$ at turn n

$$\begin{aligned}\tilde{\boldsymbol{x}}_n &= \sum_{k=0}^{n} \sin\left[2\pi\nu_b\,(n-k)\right]\boldsymbol{\Delta p}_{A,k} \\ &= \sqrt{\beta_{cc}}\frac{eV_0}{E_b}\sum_{k=0}^{n}\sin\left[2\pi\nu_b(n-k)\right]\sin\left[\hat{\phi}\cos\left(2\pi\nu_s k+\psi\right)\right]\boldsymbol{\Delta A}_k\end{aligned}$$

for a particle ζ with betatron tune ν_b, peak amplitude of the synchrotron oscillation $\hat{\phi}$ (in radians), synchrotron tune ν_s, and phase of the synchrotron oscillation at time zero ψ. In the second equation, we have expanded the momentum kick as a sinusoidal function of the particle phase deviation at turn k. See [9] for more details.

We will show that the mode 1 signal (transverse bunch tilt) measured by the pickup at turn n is proportional to the covariance of the random variables $\tilde{\boldsymbol{x}}_n$ and $\boldsymbol{\phi}_n$ (the particle longitudinal position with respect to the bunch center in radians at turn n). Let us first evaluate this covariance

$$E[\tilde{\boldsymbol{x}}_n\boldsymbol{\phi}_n] = E[\tilde{\boldsymbol{x}}_n\hat{\boldsymbol{\phi}}\cos\left(2\pi\boldsymbol{\nu}_s n+\boldsymbol{\psi}\right)].$$

Similar to Appendix B in [9],

$$\begin{aligned}
&E[\sin[2\pi\boldsymbol{\nu}_b(n-k)]\sin[\hat{\boldsymbol{\phi}}\cos(2\pi\boldsymbol{\nu}_s k+\boldsymbol{\psi})]\hat{\boldsymbol{\phi}}\cos(2\pi\boldsymbol{\nu}_s n+\boldsymbol{\psi})]\\
&\quad=E\left[\sin[2\pi\boldsymbol{\nu}_b(n-k)]\left\{2\sum_{p=0}^{\infty}(-1)^p J_{2p+1}[\hat{\boldsymbol{\phi}}]\cos[(2p+1)(2\pi\boldsymbol{\nu}_s k+\boldsymbol{\psi})]\right\}\hat{\boldsymbol{\phi}}\cos(2\pi\boldsymbol{\nu}_s n+\boldsymbol{\psi})\right]\\
&\quad=E\left[\sin[2\pi\boldsymbol{\nu}_b(n-k)]\sum_{p=0}^{\infty}(-1)^p J_{2p+1}[\hat{\boldsymbol{\phi}}]\hat{\boldsymbol{\phi}}\left\{\begin{array}{l}\cos[2\pi\boldsymbol{\nu}_s(n+2pk+k)+(2p+2)\boldsymbol{\psi}]\\+\cos[2\pi\boldsymbol{\nu}_s(-n+2pk+k)+2p\boldsymbol{\psi}]\end{array}\right\}\right].
\end{aligned}$$

We notice that the synchrotron tunespread can be neglected compared to the betatron tunespread and replace the random variable $\boldsymbol{\nu}_s$ by its mean $\overline{\nu_s}$. We get

$$\begin{aligned}
&E[\sin[2\pi\boldsymbol{\nu}_b(n-k)]\sin[\hat{\boldsymbol{\phi}}\cos(2\pi\boldsymbol{\nu}_s k+\boldsymbol{\psi})]\hat{\boldsymbol{\phi}}\cos(2\pi\boldsymbol{\nu}_s n+\boldsymbol{\psi})]\\
&\quad=E\left[\sin[2\pi\boldsymbol{\nu}_b(n-k)]\sum_{p=0}^{\infty}(-1)^p J_{2p+1}[\hat{\boldsymbol{\phi}}]\hat{\boldsymbol{\phi}}\left\{\begin{array}{l}\cos[2\pi\overline{\nu_s}(n+2pk+k)+(2p+2)\boldsymbol{\psi}]\\+\cos[2\pi\overline{\nu_s}(-n+2pk+k)+2p\boldsymbol{\psi}]\end{array}\right\}\right].
\end{aligned}$$

The random variable $\boldsymbol{\psi}$ (phase of the synchrotron oscillation) is independent of the other random variables and uniformly distributed from $-\pi$ to π. Therefore all cosine terms where the factor $\boldsymbol{\psi}$ is not zero, average to zero. Only the $p=-1$ and $p=0$ terms remain. Thus, we get

$$\begin{aligned}
&E[\sin[2\pi\boldsymbol{\nu}_b(n-k)]\sin[\hat{\boldsymbol{\phi}}\cos(2\pi\boldsymbol{\nu}_s k+\boldsymbol{\psi})]\hat{\boldsymbol{\phi}}\cos(2\pi\boldsymbol{\nu}_s n+\boldsymbol{\psi})]\\
&\quad=E[\sin[2\pi\boldsymbol{\nu}_b(n-k)]\{J_1[\hat{\boldsymbol{\phi}}]\hat{\boldsymbol{\phi}}\cos(2\pi\overline{\nu_s}[n-k])-J_{-1}[\hat{\boldsymbol{\phi}}]\hat{\boldsymbol{\phi}}\cos(2\pi\overline{\nu_s}[n-k])\}]\\
&\quad=2E\{\sin[2\pi\boldsymbol{\nu}_b(n-k)]\}E[J_1[\hat{\boldsymbol{\phi}}]\hat{\boldsymbol{\phi}}\cos(2\pi\overline{\nu_s}[n-k])],
\end{aligned}$$

where we have separated the ensemble averages over the random variables $\boldsymbol{\nu}_b$ and $\hat{\boldsymbol{\phi}}$ as they are independent. We first evaluate the ensemble average over $\hat{\boldsymbol{\phi}}$ using a Rayleigh distribution

$$E[J_1[\hat{\boldsymbol{\phi}}]\hat{\boldsymbol{\phi}}]=\int_0^{\infty}J_1[x]\frac{x^2}{{\sigma_\phi}^2}e^{-\frac{x^2}{2{\sigma_\phi}^2}}dx={\sigma_\phi}^2e^{-\frac{{\sigma_\phi}^2}{2}}.$$

Thus,

$$\begin{aligned}
E[\sin(2\pi\boldsymbol{\nu}_b(n-k))\sin[\hat{\boldsymbol{\phi}}\cos(2\pi\boldsymbol{\nu}_s k+\boldsymbol{\psi})]\hat{\boldsymbol{\phi}}\cos(2\pi\boldsymbol{\nu}_s n+\boldsymbol{\psi})]&=2{\sigma_\phi}^2e^{-\frac{{\sigma_\phi}^2}{2}}E\{\sin[2\pi\boldsymbol{\nu}_b(n-k)]\}\cos(2\pi\overline{\nu_s}[n-k])\\
&=2{\sigma_\phi}^2e^{-\frac{{\sigma_\phi}^2}{2}}h_{n-k}\cos(2\pi\overline{\nu_s}[n-k]),
\end{aligned}$$

where h_n is the impulse response of the beam transfer function. Therefore,

$$\begin{aligned}
E[\tilde{\boldsymbol{x}}_n\boldsymbol{\phi}_n]&=2\sqrt{\beta_{cc}}\frac{eV_0}{E}{\sigma_\phi}^2e^{-\frac{{\sigma_\phi}^2}{2}}\sum_{k=0}^{n}h_{n-k}\cos(2\pi\overline{\nu_s}[n-k])\boldsymbol{\Delta A}_k\\
&=2\sqrt{\beta_{cc}}\frac{eV_0}{E}{\sigma_\phi}^2e^{-\frac{{\sigma_\phi}^2}{2}}[h_n\cos(2\pi\overline{\nu_s}n)]*\boldsymbol{\Delta A}_n
\end{aligned}$$

with symbol $*$ representing the convolution. To remove normalization factors, we define the angle of an individual particle as

$$\boldsymbol{\theta}=\frac{\tilde{\boldsymbol{X}}}{\boldsymbol{z}}=\frac{\sqrt{\beta_p}\tilde{\boldsymbol{x}}}{\frac{\lambda}{2\pi}\boldsymbol{\phi}}=\frac{2\pi\sqrt{\beta_p}}{\lambda}\frac{\tilde{\boldsymbol{x}}}{\boldsymbol{\phi}},$$

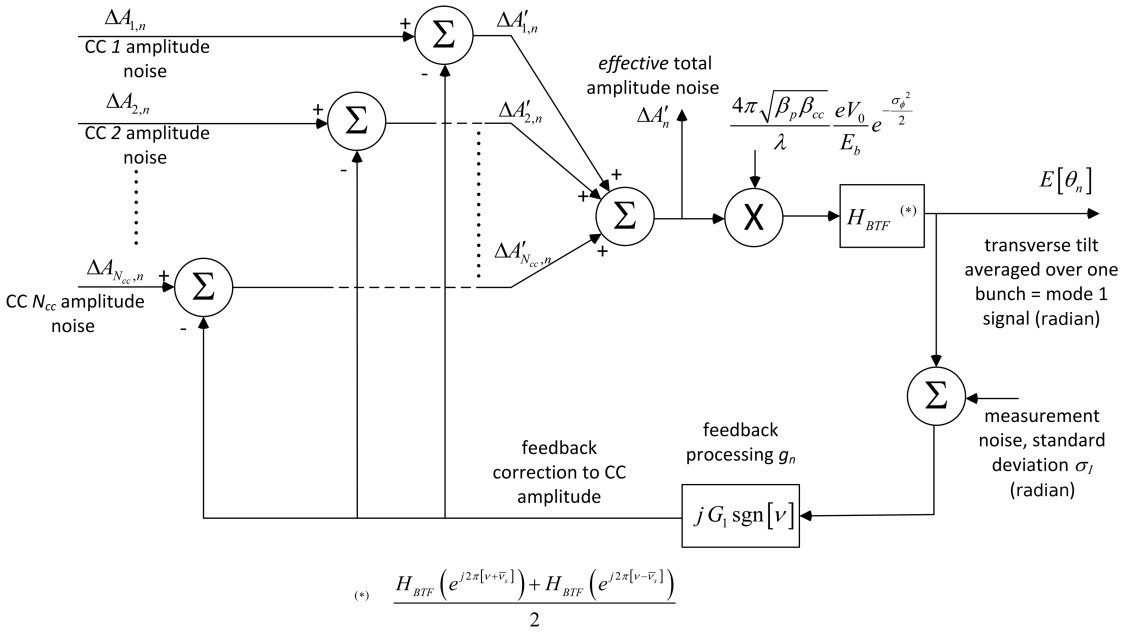

FIG. 17. Crab cavity amplitude feedback (mode 1).

where $\tilde{\boldsymbol{X}}$ is the particle transverse deviation and $\boldsymbol{z}$ its longitudinal position with respect to the bunch center, both in meter, and λ the rf wavelength. Assuming that $\tilde{\boldsymbol{x}}$ and $\boldsymbol{\phi}$ are jointly Gaussian (zero mean), the tilt $\boldsymbol{\theta}$ is Cauchy distributed with mean [38]

$$E[\boldsymbol{\theta}] \triangleq \frac{2\pi\sqrt{\beta_p}}{\lambda} E\left[\frac{\tilde{\boldsymbol{x}}}{\boldsymbol{\phi}}\right] = \frac{2\pi\sqrt{\beta_p}}{\lambda}\frac{E[\tilde{\boldsymbol{x}}\boldsymbol{\phi}]}{\sigma_\phi^2}$$

and then

$$\begin{aligned} E[\boldsymbol{\theta}_n] &= \frac{2\pi\sqrt{\beta_p}}{\lambda}\frac{2}{\sigma_\phi^2}\sqrt{\beta_{cc}}\frac{eV_0}{E}{\sigma_\phi}^2 e^{-\frac{\sigma_\phi^2}{2}}[h_n\cos(2\pi\overline{\nu_s}n)] * \boldsymbol{\Delta A}_n \\ &= \frac{4\pi\sqrt{\beta_{cc}\beta_p}}{\lambda}\frac{eV_0}{E}e^{-\frac{\sigma_\phi^2}{2}}[h_n\cos(2\pi\overline{\nu_s}n)] * \boldsymbol{\Delta A}_n. \end{aligned} \quad \text{(B1)}$$

The mode 1 measurement (average tilt) is the convolution of the amplitude noise process with the impulse response of the beam transfer function *modulated* by the synchrotron tune. The effect of the synchrotron tune is not surprising. It appears in Eq. (2) above: the beam is sensitive to the part of the amplitude noise spectrum overlapping the betatron tune distribution but *shifted* up or down by the synchrotron tune. As a particle moves from the head to the tail of the bunch at the synchrotron frequency, amplitude noise at $\nu_b \pm \nu_s$ will result in kicking a given particle at the ν_b frequency and thus in a resonant response. In the frequency domain, the modulation of the beam transfer function results in shift by $\pm\overline{\nu_s}$ (Fig. 17). The feedback correction is proportional to the pickup mode 1 (tilt) measurement, with a 90° phase shift. It is applied to the voltage set point of all N_{cc} cavities, assumed as having identical V_0 voltage. Let $\boldsymbol{\Delta A}_n$ be the sum of the amplitude noise from the N_{cc} cavities. The crab cavity feedback loop modifies $\boldsymbol{\Delta A}_n$, resulting in the *effective* amplitude noise $\boldsymbol{\Delta A}'_n$, with a PSD varying within the tunespread. At tune ν_b (and its revolution frequency aliases), the effect of the crab cavity amplitude noise will be reduced, in PSD, by the square modulus of the closed loop response:

$$\begin{aligned} R_A(\nu_b) &= \frac{S_{\Delta A'}[(k+\nu_b)f_{\mathrm{rev}}]}{S_{\Delta A}[(k+\nu_b)f_{\mathrm{rev}}]} \\ &= \frac{1}{\left|1 + jG_1N_{cc}\frac{2\pi\sqrt{\beta_{cc}\beta_p}}{\lambda}\frac{eV_0}{E}e^{-\frac{\sigma_\phi^2}{2}}\left[H_{\mathrm{BTF}}(e^{j2\pi[\nu_b+\overline{\nu_s}]}) + H_{\mathrm{BTF}}(e^{j2\pi[\nu_b-\overline{\nu_s}]})\right]\right|^2}. \end{aligned} \quad \text{(B2)}$$

[1] R. Calaga, Crab cavities for the LHC upgrade, in *Proceedings of Chamonix 2012 workshop on LHC Performance* (2012), https://cds.cern.ch/record/1424362.

[2] High-luminosity large hadron collider: Technical design report, CERN Report No. CERN-2017-007-M, 2017.

[3] K. Oide and K. Yokoya, Beam-beam collision scheme for storage-ring colliders, Phys. Rev. A **40**, 315 (1989).

[4] Y. Funakoshi (KEKB Commissioning Group), Operational experience with crab cavities at KEKB, in *Proceedings, ICFA Mini-Workshop on Beam-Beam Effects in Hadron Colliders, BB2013* (CERN, Geneva, Switzerland, 2014), pp. 27–36.

[5] T. Abe *et al.*, Compensation of the crossing angle with crab cavities at KEKB, in *Proceedings of the 22nd Particle Accelerator Conference, PAC-2007, Albuquerque, NM* (IEEE, New York, 2007); *Conf. Proc.* C070625, 27 (2007).

[6] K. Hosoyama *et al.*, Development of the KEK-B Superconducting Crab Cavity, in *Proceedings of the 11th European Particle Accelerator Conference, Genoa, Italy, 2008* (EPSAG, Geneva, 2008); *Conf. Proc.* C0806233, THXM02 (2008).

[7] E. Yamakawa, R. Apsimon, P. Baudrenghien, R. Calaga, and A. Dexter, Luminosity reduction caused by phase modulations at the HL-LHC crab cavities, Nucl. Instrum. Methods Phys. Res., Sect. A **908**, 338 (2018).

[8] K. Ohmi *et al.*, Response of colliding beam-beam system to harmonic excitation due to crab-cavity rf phase modulation, Phys. Rev. ST Accel. Beams **14**, 111003 (2011).

[9] P. Baudrenghien and T. Mastoridis, Transverse emittance growth due to rf noise in the high-luminosity lhc crab cavities, Phys. Rev. ST Accel. Beams **18**, 101001 (2015).

[10] J. Qiang, G. Arduini, J. Barranco, Y. Papaphilippou, and T. Pieloni, Beam-beam simulation of crab cavity with frequency dependent noise for LHC upgrade, in *Proceedings of the 7th International Particle Accelerator Conference, IPAC 2016, Busan, Korea* (JACoW, Geneva, Switzerland, 2016), TUPOR017.

[11] A. Alekou, R. Appleby, H. Bartosik, R. Calaga, M. Carla, and Y. Papaphilippou, SPS long term stability studies in the presence of crab cavities and high order multipoles, in *Proceedings of the 61st ICFA Advanced Beam Dynamics Workshop (HB-2018), Daejeon, Korea, 2018* (JACoW, Geneva, Switzerland, 2018), pp. 284–286, 10.18429/JACoW-HB2018-WEP2PO008.

[12] P. Baudrenghien, T. Mastoridis, and E. Yamakawa, SPS LLRF measurements and lessons learned, in *Proceedings of the 8th HL-LHC Collaboration Meeting, CERN, Geneva, Switzerland* (2018), https://indico.cern.ch/event/742082/.

[13] Y. Alexahin, On the Landau damping and decoherence of transverse dipole oscillations in colliding beams, Part. Accel. **59**, 43 (1998), https://cds.cern.ch/record/314169.

[14] Y. Alexahin, On the emittance growth due to noise in hadron colliders and methods of its suppression, Nucl. Instrum. Methods Phys. Res., Sect. A **391**, 73 (1997).

[15] X. Buffat, Suppression of emittance growth by a collective force: Van Kampen approach, in *Proceedings of the 13th International Particle Accelerator Conference, Bangkok, Thailand* (JACoW, Geneva, Switzerland, 2022).

[16] N. Triantafyllou, F. Antoniou, H. Bartosik, P. Baudrenghien, X. Buffat, R. Calaga, L. R. Carver, T. Mastoridis, Y. Papaphilippou, and A. Wolski, Investigation of damping effects of the crab cavity noise induced emittance growth, in *Proceedings of the 12th International Particle Accelerator Conference, IPAC-2021, Campinas, SP, Brazil* (JACoW, Geneva, Switzerland, 2021), p. 2054.

[17] N. Triantafyllou, F. Antoniou, H. Bartosik, P. Baudrenghien, X. Buffat, R. Calaga, T. Mastoridis, Y. Papaphilippou, and A. Wolski, Suppression of crab cavity noise induced emittance growth by transverse beam coupling impedance, in *Proceedings of the 13th International Particle Accelerator Conference, Bangkok, Thailand* (JACoW, Geneva, Switzerland, 2022), WEOZSP2.

[18] N. Triantafyllou, H. Bartosik, P. Baudrenghien, X. Buffat, R. Calaga, Y. Papaphilippou, and A. Wolski, Impact of beam coupling impedance on crab cavity noise induced emittance growth (to be published).

[19] X. Buffat, W. Herr, T. Pieloni, and D. Valuch, Modeling of the emittance growth due to decoherence in collision at the large hadron collider, Phys. Rev. Accel. Beams **23**, 021002 (2020).

[20] G. Arduini *et al.*, HL-LHC run 4 proton operational scenario, CERN Report No. CERN-ACC-2022-0001, 2022.

[21] E. Metral *et al.*, Update of the HL-LHC operational scenarios for proton operation, CERN Report No. CERN-ACC-NOTE-2018-0002, 2019.

[22] E. Metral, Run 4 operational scenario (p+) and status of optics v1.6, in *Proceedings of the 12th HL-LHC Collaboration Meeting, Uppsala, Sweden* (2022), https://indico.cern.ch/event/1161569/.

[23] P. Baudrenghien and T. Mastoridis, HL-LHC crab cavity field regulation and resulting RF noise spectrum, CERN Report No. CERN-ACC-NOTE-2023-0006, 2023.

[24] A. Spierer, P. Baudrenghien, J. Egli, G. Hagmann, P. Kuzmanovic, I. Stachon, M. Suminski, and T. Wlostowski, The CERN SPS low level RF: The beam control, in *Proceedings of the 13th International Particle Accelerator Conference, Bangkok, Thailand* (JACoW, Geneva, Switzerland, 2022).

[25] G. Hagmann, P. Baudrenghien, J. Egli, A. Spierer, M. Suminski, and T. Wlostowski, The CERN SPS low level RF: The beam-control, in *Proceedings of the 13th International Particle Accelerator Conference, Bangkok, Thailand* (JACoW, Geneva, Switzerland, 2022).

[26] P. Baudrenghien *et al.*, The LHC Low Level RF, in *Proceedings of the 10th European Particle Accelerator Conference, Edinburgh, Scotland, 2006* (EPS-AG, Edinburgh, Scotland, 2006), pp. 1471–1473.

[27] The random variable $\boldsymbol{\psi}$ (the betatron oscillation phase) is uniformly distributed from $-\pi$ to π and independent of the other variables. $\boldsymbol{\nu}_b$ and $\hat{\boldsymbol{\phi}}$ are independent. We assume two-dimensional Gaussian distribution in longitudinal phase space resulting in the random variable $\hat{\boldsymbol{\phi}}$ being Rayleigh distributed.

[28] G. Kotzian, Possibilities for transverse feedback phase adjustment by means of digital filters, J. Phys. Conf. Ser. **874**, 012089 (2017).

[29] A. Chao, *Physics of Collective Beam Instabilities in High Energy Accelerators*, Wiley Series in Beam Physics and Accelerator Technology (Wiley-Interscience, New York, 1993).

[30] A. W. Chao and M. Tigner, *Handbook of Accelerator Physics and Engineering*, 1st ed. (World Scientific, Singapore, 1999).

[31] V. Lebedev, V. Parkhomchuk, V. Shiltsev, and G. Stupakov, Emittance growth due to noise and its suppression with the feedback system in large hadron colliders, Superconducting Super Collider Laboratory (SSCL) Report No. SSCL-PREPRINT-188, 1993.

[32] V. Lebedev, Emittance growth due to noise and its suppression with the feedback system in large hadron colliders, AIP Conf. Proc. **326**, 396 (1995).

[33] W. Höfle *et al.*, Transverse damping systems for the future CERN LHC, in *Proceedings of the 19th Particle Accelerator Conference, Chicago, IL, 2001* (IEEE, Piscataway, NJ, 2001), pp. 1237–1239.

[34] G. Rumolo, Practical user guide for headtail, CERN Report No. CERN-SL-Note-2002-036.

[35] G. Rumolo and F. Zimmermann, Electron cloud simulations: beam instabilities and wakefields, Phys. Rev. ST Accel. Beams **5**, 121002 (2002).

[36] P. Baudrenghien, T. Mastoridis, and B. Miller, Crab cavity RF noise feedback and transverse damper interaction, CERN Report No. CERN-ACC-NOTE-2019-0006, 2019.

[37] D. Valuch and V. Stopjakova, New generation of very low noise beam position measurement system for the LHC transverse feedback, in *Proceedings of the 13th International Particle Accelerator Conference, Bangkok, Thailand* (JACoW, Geneva, Switzerland, 2022).

[38] A. Papoulis and S. U. Pillai, *Probability, Random Variables, and Stochastic Processes*, McGraw-Hill Series in Electrical and Computer Engineering (McGraw-Hill, New York, 2002), https://books.google.com/books?id=k22UwAEACAAJ.